THE EFFECT OF STATIC AND RESIDUAL STRESSES ON GRAPHITIC CORROSION

A THESIS

Presented to

The Faculty of the Division

of Graduate Studies

By

Efstathios I. Meletis

In Partial Fulfillment

of the Requirements for the Degree

Master of Science in Chemical Engineering

Georgia Institute of Technology

May, 1978

THE EFFECT OF STATIC AND RESIDUAL STRESSES

ON GRAPHITIC CORROSION

Approved:

Robert Hochman, Chairman

H. E. Grenga

Pieter Muijen

Date approved by Chairman: _____

THIS IS DEDICATED TO MY FAMILY

ACKNOWLEDGMENTS

The author wishes to express his sincere appreciation to his thesis advisor, Dr. R. F. Hochman, who suggested this research project and contributed invaluable aid during the entire course of the work. He is greatly indebted to Dr. H. E. Grenga and Dr. P. Muije for having taken time to review this work and for their constructive criticism.

Sincere thanks are extended to Dr. M. Marek, who helped considerably in experimental problems encountered during this work.

The author also wishes to thank Mr. C. Blackwood and the graduate students, J. G. Rinker and D. Averette, who gave freely of their time and energy.

TABLE OF CONTENTS

	Page
ACKNOWLEDGMENTS	ii
LIST OF TABLES	iv
LIST OF ILLUSTRATIONS	v
SUMMARY	viii
Chapter	
I. INTRODUCTION	1
II. THEORY	5
Cast Irons Graphitization or Graphitic Corrosion Corrosive Soils Corrosion Mechanism Galvanic Effects Localized Graphitization Corrosion The Effect of Res.Str. and Static Load on Graphitic Corrosion	
III. EXPERIMENTAL	18
Apparatus Specimens Experimental Procedure Potentiostatic Measurements	
IV. RESULTS AND DISCUSSION OF RESULTS	33
Polarization Measurements Graphitic Corrosion Measurements Evaluation of the Graphitic Corrosion	
V. CONCLUSIONS	68
VI. RECOMMENDATIONS	69
APPENDICES	70
BIBLIOGRAPHY	77

LIST OF TABLES

Table		Page
1.	Composition of the Two Types of the Tested Cast Iron.	21
2.	Phase I Experimental Conditions.	27
3.	Phase II Experimental Conditions	28
4.	Phase III Experimental Conditions.	29
5.	Galvanic Couples Tested.	30
6.	Open Circuit Potentials and Corrosion Potentials and Currents for the Five Galvanic Couples.	34
7.	Exposure Time, Maximum and Average Penetration and Penetration Rate for Phase I Experiments, For Material A and Material B.	39
8.	Exposure Times (Times to Failure), Maximum and Average Penetration and Penetration Rates for Phase II Experiments, for Material A and Material B	41
9.	Ratio of Maximum Penetration Rates of Phase II to Phase I Experiments	58
10.	Ratio of the Maximum Corrosion Penetration Rate Between Phase II and Phase I Case I Experiments.	59
11.	Exposure Times to Failure, Maximum and Average Penetrations and Penetration Rates for Three Stress Values with No Impressed Current, of Material A and Material B of Phase III Experiments.	61
12.	Exposure Time to Failure, Maximum and Average Penetrations and Penetration Rates for Three Stress Values with an Impressed Current, of Material A and Material B of Phase III Experiments.	65

LIST OF ILLUSTRATIONS

Figure		Page
1.	General View of a Typical "Finger-Like" Graphitization Attack on Centrifugally Cast, Cast Iron Pipe.	4
2.	23X Magnification. Unetched--Photomicrograph of Localized Graphitization Corrosion	4
3.	Schematic Diagram of the Apparatus Showing the Specimen Loading Location and the Critical Dimensions	19
4.	100X Magnification. Unetched Microstructure of Material A	22
5.	100X Magnification. Unetched Microstructure of Material B	22
6.	The Arrangement of the Specimen, Cup, Graphite Cathode and Battery During the Application of An External Potential.	25
7.	A Polarization Diagram Representation of Initial (1) and Final (2) Conditions for Voltage Application	26
8.	Schematic Drawing of the Cells; (a) Cell for the Potential Difference Measurements, (b) Cell for the Detection of the Variation in Corrosion Potential and Current Versus Time . .	32
9.	Corrosion Potential as a Function of Time for the Five Galvanic Couples	35
10.	Corrosion Currents as a Function of Time for the Five Galvanic Couples	36
11.	Combined Activation Polarization Curves for the Five Galvanic Couples	37
12.	Maximum Penetration Versus Time for Case I of Phase II	42
13.	Maximum Penetration Versus Time for Case II of Phase II	43

Figure Page

14. Maximum Penetration Versus Time for Case III of Phase II. 44

15. Maximum Penetration Versus Time for Case IV of Phase II. 45

16. Average Penetration Versus Time for Case I of Phase II. 46

17. Average Penetration Versus Time for Case II of Phase II. 47

18. Average Penetration Versus Time for Case III of Phase II. 48

19. Average Penetration Versus Time for Case IV of Phase II. 49

20. Maximum Penetration Rate Versus Time for Case I of Phase II 50

21. Maximum Penetration Rate Versus Time for Case II of Phase II. 51

22. Maximum Penetration Rate Versus Time for Case III of Phase II 52

23. Maximum Penetration Rate Versus Time for Case IV of Phase II. 53

24. Average Penetration Rate Versus Time for Case I of Phase II 54

25. Average Penetration Rate Versus Time for Case II of Phase II. 55

26. Average Penetration Rate Versus Time for Case III of Phase II 56

27. Average Penetration Rate Versus Time for Case IV of Phase II. 57

28. Maximum Penetration Rate Versus Stress for Material A and B 62

29. Average Penetration Rate Versus Stress for Materials A and B. 63

30. Maximum Penetration Rate Versus Stress (with Applied Potential of 0.2 V) for Materials A and B. 66

Figure Page

31. Average Penetration Rate Versus Stress (with Applied Potential of 0.2 V) for Materials A and B. 67

SUMMARY

This research was conducted principally to determine the effect of applied stress, residual stresses and induced current on graphitic corrosion and to investigate the relation of these variables to highly localized graphitic corrosion attack of centrifugally cast, cast iron.

Cast iron specimens with and without residual stresses and with and without an applied potential were exposed and tested under static stress, in a 3.5 percent sodium chloride solution of pH 3. The initial corrosion tests were followed by polarization measurements and studies under accurate stress conditions.

The results showed that residual stresses have a small effect on the graphitic corrosion rate. The static stresses coupled with residual stresses and combined with low potential differences highly accelerated the corrosion rate and resulted in highly localized graphitic corrosion attacks. A significant determination of the study was a critical stress value, approximately 70 percent of the tensile strength, above which the graphitic corrosion rate became extremely high in localized high stress areas.

CHAPTER I

INTRODUCTION

The main purpose of this research was to investigate the metallurgical and corrosion factors which lead to graphitization rates one or two orders of magnitude greater than normal graphitization corrosion rates for centrifugally cast, cast iron pipe. The localized "finger-like or fissure" graphitization corrosion attack has been the cause of a number of gas line explosions. Because of the time dependency of the highly localized nature of this type of attack, a steadily increasing number of these failures are occurring and apparently will continue to occur.

It is well known that cast iron exposed to various types of environments, including certain soils, suffers from corrosion damage called graphitization. However, only little scientific analysis and examination of the problem has been made and literature dealing with fundamental aspects of the problem [2,3,4,5,6,7], is limited. In general, in this type of corrosion the ferrite of the cast iron is removed from the attacked area leaving behind a black porous layer consisting of graphite and carbides. The mechanism of this reaction involves the formation of galvanic cells, in which the ferrite acts as an anode and dissolves in the

solution and the more noble graphite acts as the cathode. The graphitized layer may decrease or prevent the corrosion of the remaining cast iron metal when the graphitic layer has reached a diffusion limiting thickness [5] if its pores are filled with residual solid corrosion products. However, if the layer remains porous acceleration of the corrosion attack may occur due to the presence of a large graphite surface to act as a cathode. The occurence of localized or fissure corrosion indicates that possibly the graphite-rich layer has been locally disturbed, allowing the corrosive solution to penetrate and reach the inner metallic surface. With the enlargement of the exposed graphite area with comparison to the metal resulted in accelerated attack of the base metal. This may be a result of static and/or residual stresses in centrifugal cast, cast iron.

The present study was initiated to determine the effect of static loads, residual stresses and localized currents on graphitization.

One set of specimens of centrifugally cast, cast iron with and without residual stresses was exposed in a 3.5 percent sodium chloride solution. Specimens from another set were stressed in three-point bending, some of these were locally heated to develop residual stresses. Accelerated corrosion conditions were provided in some tests by potentiostatic anodic polarization. Finally specimens at various stress levels, selected as a percentage of the

fracture stress, were tested. The corrosive solution for the three phases was 3.5 percent NaCl with pH of 3.

Results showed that static stress can increase the corrosion rate up to 50 times. Static applied stress plus residual stresses can increase the corrosion rate up to 60 times and one or both plus an impressed current can easily accelerate the corrosion rate 100 times that of the normal graphitic corrosion rate.

Microscopic examination indicated localized corrosion attacks and breakdown of the graphitic layer in the area of the maximum stress. This permitted the electrolyte to reach the inner metallic surface and accelerate and localize graphitic corrosion.

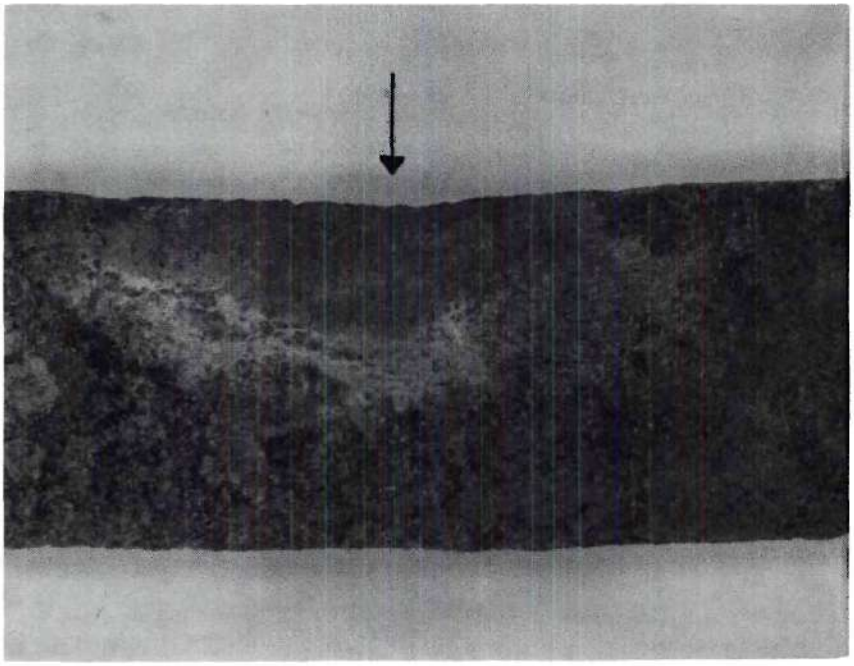

Figure 1. General View of a Typical "Finger-Like" Graphitization Attack on Centrifugally Cast, Cast Iron Pipe

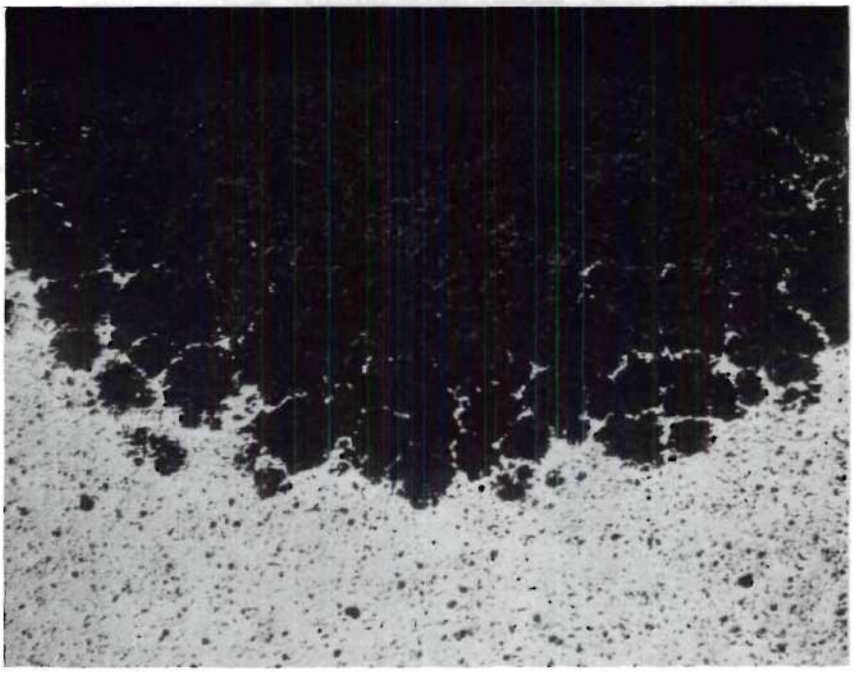

Figure 2. 23X Magnification. Unetched--Photomicrograph of Localized Graphitization Corrosion

CHAPTER II

THEORY

Cast Irons

Cast irons used in gas distribution systems are iron base alloys containing between 2.50 and 4.00 percent total carbon, from 0.50 to 3.00 percent silicon, some sulfur, phosphorus and manganese. The usual microstructure of gray cast irons is a matrix of pearlite with graphite (graphitic flakes or modules) dispersed throughout.

The mechanical properties of cast iron [1] depend to a great extent upon the amount, size, shape, and distribution of the graphite and the characteristics of the steel-like matrix. Because of the high carbon content, they are brittle and have a low ductility. There are four primary types: (a) white, (b) gray, (d) malleable and nodular cast iron.

The molting of cast iron [8] can be sand molding in which the sand is used in a moist or in a dry state. Loam molds are used also in certain cases. Other mold forms are permanent or long life molds. Centrifugally cast pipe, made in all-metal molds, is one type of permanent mold used. Centrifugal casting is a special form of casting [9] in which the molds are rotated rapidly around a vertical or

horizontal axis. While the metal is poured, the mold is forcing the metal to the sides of the mold by centrifugal force. The above procedure is an especially effective way of making pipe.

Graphitization or Graphitic Corrosion

Graphitization was a term used for selective corrosion of cast irons but is now restricted strictly to the microstructural change [1] which occurs in white and to some extent other cast irons, when they are heated to moderate temperatures, or the basic decompositions of cementite into ferrite and carbon (graphite):

$$Fe_3C \rightarrow 3Fe + C \text{ (graphite)}$$

during normal cooling.

Graphitic corrosion often called graphitization is a type of selective leaching (a form of disintegration) which cast iron suffers, when exposed to certain types of corrosive environments. Because of the variation (inhomogeneity) in composition of cast iron and the electrical contact in an electrolyte between graphite and ferrite or ferrite and iron carbide, formation of galvanic cells takes place [2], which lead to electrochemical action between these two constituents. The less noble ferrite (anode) is attacked selectively by the more noble graphite (cathode). In

graphitic corrosion much of the ferrite of the cast iron is dissolved from the affected zones into the solution, leaving behind a black porous mass. This porous material is residual graphite which also contains some carbides and variable amounts of free iron and iron oxide.

The graphitic corrosion usually occurs at a low rate although the black porous mass is very weak. The change in the metal thickness is negligible and the corroded surface does not appear different from main metal.

Highly localized (fissure-type) graphitization attack has been observed in gray cast iron, more often in centrifugal cast, cast iron pipes, and has been the cause of a number of gas explosions. Graphitization rates, 100 times the normal graphitization corrosion rate can occur and may be caused by stress or special environmental conditions, but these factors have not been identified as yet. Obviously hundreds of miles of cast iron gas line still exist although it has been phased out of use as a line material. Because of the time dependency and the highly localized nature of this type of attack, a steadily increasing number of these cast iron gas line failures are occuring.

Corrosive Soils

The soil is a very important determining factor in the corrosion of cast iron in underground uses. Soils differ radically in their corrosive action on cast iron and soils

which are potentially aggresive to cast iron are infrequent. A corrosive soil [4] must generally have a pH below 4.0 acidity or above 12 alkalinity or high concentrations of soluble salts (low electrical resistivity) or it must be in areas where stray currents are present.

Other factors influencing the corrosive ability of the soils [6,7] are, differential aerations which may result from local differences in packing of the soil, variations in the moisture and oxygen content and permeability of the soil to moisture and oxygen. The term permeability contains physical characteristics of the soil such as particle size, specific gravity, particle distribution and the shrinkage which occurs when wet soil dries. It has been found that the commonly used cast-iron pipe corrodes at nearly the same rate in the same soil environment. Generally the rate of corrosion is controlled by the properties and characteristics of the soils and varies widely in different soils. However, some of the unique localized graphitic corrosion effects can not be directly related to soil differences.

Corrosion Mechanism

It is generally agreed that the contact between the ferrite or ferrite-pearlite and the graphite in the cast iron structure leads to electrochemical action between these constituents, because of the potential difference between matrix and graphite. It is also understood that the

presence of an electrolyte is necessary for the reaction to occur.

Under these conditions the corrosion reaction [3] involves a current flow between the attacked areas from the metal (anode) though the electrolyte to the graphite flakes (cathode) and then through the graphite to the metal to complete the circuit. The carbon existing as graphite or carbides in most soils is more noble than the iron matrix therefore acts as cathode in the corrosion current circuit.

The principal electrochemical reactions which occur at the cathodes are:

(a) the discharge of hydrogen ions and the evolution of hydrogen as a gas. For this reaction to occur high hydrogen ion concentration and potential difference required.

(b) If the above reasons are not satisfied the cathodic reaction can involve some reaction with oxygen. This oxygen reaction could be a combination of the discharge of hydrogen ions with oxygen to give water, hydrogen peroxide or cathodic reduction of oxygen to give hydroxyl ions.

The anodic reaction involves the dissolution of the ferritic matrix. As the reaction proceeds the oxygen, which is dissolved in the solution, is consumed. The ferritic matrix dissolves and most of the corrosion products are

removed by the solution. However, the flakes of residual graphite accumulate on the surface. As the oxygen is consumed during the corrosion reaction the amount of oxygen remaining in the electrolyte will have a controlling effect on the reaction. In most soils there are certain bacteria with oxidizing effects which can replace oxygen from the cathodic reaction. If the amount of oxygen is sufficient, the corrosion reaction and the accumulation of graphite flakes proceeds, and the thickness of the porous graphitic layer increases.

After some time the solution can no longer reach the inner metallic surface because the graphite network behaves as a barrier against the diffusion of oxygen into the graphite layer.

Under these conditions a differential aeration cell is formed where the external surface is cathodic and the internal surface of the pit or remain metal surface is anodic. It is common for metals to suffer from corrosion currents that have their source in differences in the corrosive nature of the environment at different areas on the metal surface. Such effects are often found in underground piping systems. For example, if a pipe of cast iron [7] passes through two soils of different composition that differ in oxygen concentration, a current will flow from the more poorly aerated area (anode) through the soil to the better aerated area (cathode) and back through the pipe to the anodic

area. This is analogous to a concentration cell.

It is easy to understand then, that bulk graphitic corrosion is primarily due to electrochemical action between the ferritic and graphitic constituents of cast iron and perhaps in some cases partly from differential aeration cells in the soil.

The factor which determines the corrosion rate [3] is the current density. The rates of the electrochemical reactions at the anodes and cathodes are proportional to the current density. It is obvious that the size and distribution of anodic and cathodic areas are very important because they determine the current density for a fixed total amount of current.

The cathodic reaction is balanced by the anodic iron matrix dissolution. As the reaction proceeds [5] the concentration of Fe^{++} is higher at the anodic area than the concentration of ferrous ions towards the external cathodic area. In this case the gradient of chemical and electrical potential contribute to increase the electrochemical potential which results in migration of ferrous ions from the vicinity of anodic area towards the cathodic area. The ferrous ions, coming out of the graphitic porous layer, diffuse through the limiting layer into the solution forming oxidation products, which are removed by the solution.

If hydroxyl ions are produced by the cathodic

reduction, they may penetrate the graphitic layer and react with the ferrous ions leaving the area to give iron hydroxides, which will precipitate and accumulate in the porous graphite layer. Under these conditions the gradient of the electrochemical potential promotes the migration of the hydroxyl ions from the external surface into the porous graphitic layer. This precipitation causes an increase of the electrical potential of the solution which is into the graphitic layer, followed by a decrease of the electrochemical potential.

The precipitation of oxidation products within the graphite layer depends on the following factors:

(a) The structure of the cast iron. The residual graphite flakes, after the dissolution of iron matrix, form a porous graphite network with very good electrical contact between particles of graphite. In such a layer the electrical resistance of the graphite layer and of the solution within the porous layer are very small.

(b) The chemical composition of cast iron. When the cast iron contains nickel the oxidation potential of ferrous ions can be easily accomplished, because the dissolution potential of the matrix becomes more noble than the one of iron.

(c) The chemical reactivity and concentration of the solution. If the corrosive solution is diluted, the solution inside the graphite layer will be more diluted and

this results in an increase in electrical resistance of the solution within the porous layer, causing the precipitation of protective oxides. Protective graphitic corrosion products are most likely to be encountered in neutral and alkaline environments and least likely in acid solutions.

(d) The environmental conditions. The environmental conditions determine the ability of graphitic corrosion products to adhere to the corroded iron surface. Adherence to the point of building up graphitic layers of substantial thickness are expected where the surfaces are regularly or frequently subjected to abrasion or erosion, which remove the graphite particles as fast as they become exposed. On the other hand, burial in the earth or exposure to liquids in relatively quiet conditions will favor acculumation of layers of graphitic corrosion products. The velocity of the external solution flow determines the thickness of the limiting diffusion layer. For a determined thickness of diffusion layer, the aeration of the external solution determines the flow of oxygen and finally the value of the corrosion current.

(e) Thickness of the graphitized layer. As the thickness of the graphitic layer increases the electrical resistance of the graphitic layer and of the solution within the layer increases. So the graphitic corrosion vanishes and stops spontaneously after a determined thickness of the graphitized layer has been reached, except for the highly

localized or fissure corrosion which is now being observed relatively often.

Galvanic Effects

When other metals are in electrical contact with cast iron in an electrolyte, galvanic corrosion takes place. The galvanic corrosion can often be recognized by the fact that the corrosion is more severe [1] near the junction of the two metals than elsewhere on the metal surfaces. The greater the difference in potential between the two metals, the greater the probability the galvanic attack will be severe. The corrosion situation depends on the relative noble active relation between the metals forming the galvanic couple. If the cast iron [5] is less noble than the other metal which is often the case, then the cast iron becomes the anode and the other material cathode and dissolution of the iron matrix of cast iron takes place. The intensity of these effects will be influenced by the size of the cathodic and anodic area, the distance between the areas, the metals involved and the electrical resistance of the galvanic circuits, including that of the electrolyte, in which the reactions are occuring.

If the graphitized cast iron is more noble the cathodic role of the graphite layer can stimulate the corrosion process of the other metal.

Under these conditions a clogging of the pores of

the graphite layer may be beneficial in avoiding corrosion of the underlying iron but it also serves to increase the galvanic acceleration of corrosion of clean metal with which may be in contact with it in a corrosion solution.

Localized Graphitization Corrosion

The localized graphitization corrosion of cast iron is a case where the graphitic corrosion rate may be a hundred-times the normal graphitization corrosion rates. This indicates that the corrosion of cast iron can be influenced by some form of accelerating condition or conditions, e.g., the galvanic effect between graphite and cast iron.

During the graphitic corrosion, if the graphite layer remains porous it accelerates the corrosion of the cast iron base and the thickening of the layer tends to provide an increasingly large cathodic area of graphite surface due to its porous structure. The galvanic effect of the contact of the base metal with the large area of graphite [2] may cause the cast iron to corrode much more rapidly. The higher the graphite/metal ratio the greater the localized corrosion. It is also common knowledge that in underground uses of cast iron the corrosion rate is affected by the soil properties, and the kind and concentration of soluble salts in the soils. In pipeline service systems which actually run for considerable distances transverse soils of varying composition, aeration and moisture content giving rise to long line

currents which potentially affect the corrosion rate.

The occurrence of highly localized or fissure corrosion shows that probably the graphite rich layer has been locally disturbed. Under these conditions the electrolyte is allowed to penetrate to reach the metal and to continue the corrosion reaction. Some of these possibilities are being explored as the subject of this thesis.

The Effect of Res.Str. and Static Load on Graphitic Corrosion

Residual stresses, which can have a profound effect on the mechanical properties of a material, develop in practically all cast components during solidification [10, 11]. These stresses are usually too low to be significant, but sometimes they can reach relatively high levels, and in extreme cases may be sufficent to crack the casting, even in the absence of any external load. In practice, even the most simple shapes do not cool uniformly, since free surfaces and edges cool more rapidly than central areas. This leads to the development of differential strains. It has been shown that generally tensile forces will be developed in heavier sections and compressive forces in thinner sections.

The microstructure along the localized or fissure attack indicates that it follows the path of the columnar structure from the surface in centrifugally cast materials.

This structure shows a relationship to the thermal gradients in solidification, the chemical inhomogeneities and residual stresses that may result.

When stress is applied to cast iron the distorted high-energy zone serves as an anode, while the strain or stress free region is the cathode. This type of cell can accelerate graphitic corrosion. Application of stress on cast iron may cause a local change or crack in the graphitic layer, permitting the electrolyte and the oxygen in the electrolyte to reach the inner metallic surface. This is more prevelent in centrifugally cast, cast iron.

This breakdown of the graphite layer, due to stress or to special environmental conditions, will result in the loss of mechanical strength under relatively low static stress when coupled with corrosion conditions.

CHAPTER III

EXPERIMENTAL

This research program was conducted in three phases.

1. The first phase was a study of regular corrosion attack on two kinds of cast iron. The results of this stage of research was used as a basis for evaluation of the results of the next two phases.

2. The second phase was research on the effect of three factors, static stress, residual stresses, current and the combinations of these on the graphitic corrosion of cast iron.

3. The last research stage was a series of accurate tests in which different static stress values, were applied to specimens in the same physical and chemical conditions in order to determine the way graphitic corrosion depends on the level of static load. In addition tests of the combined effect of current and static load on corrosion was studied for a broader evaluation of the problem.

Apparatus

For the first phase of the experiments no apparatus was used. The experiments of the second and third phase were carried out in the same mechanical test unit. A schematic diagram of the apparatus used is given in Figure 3.

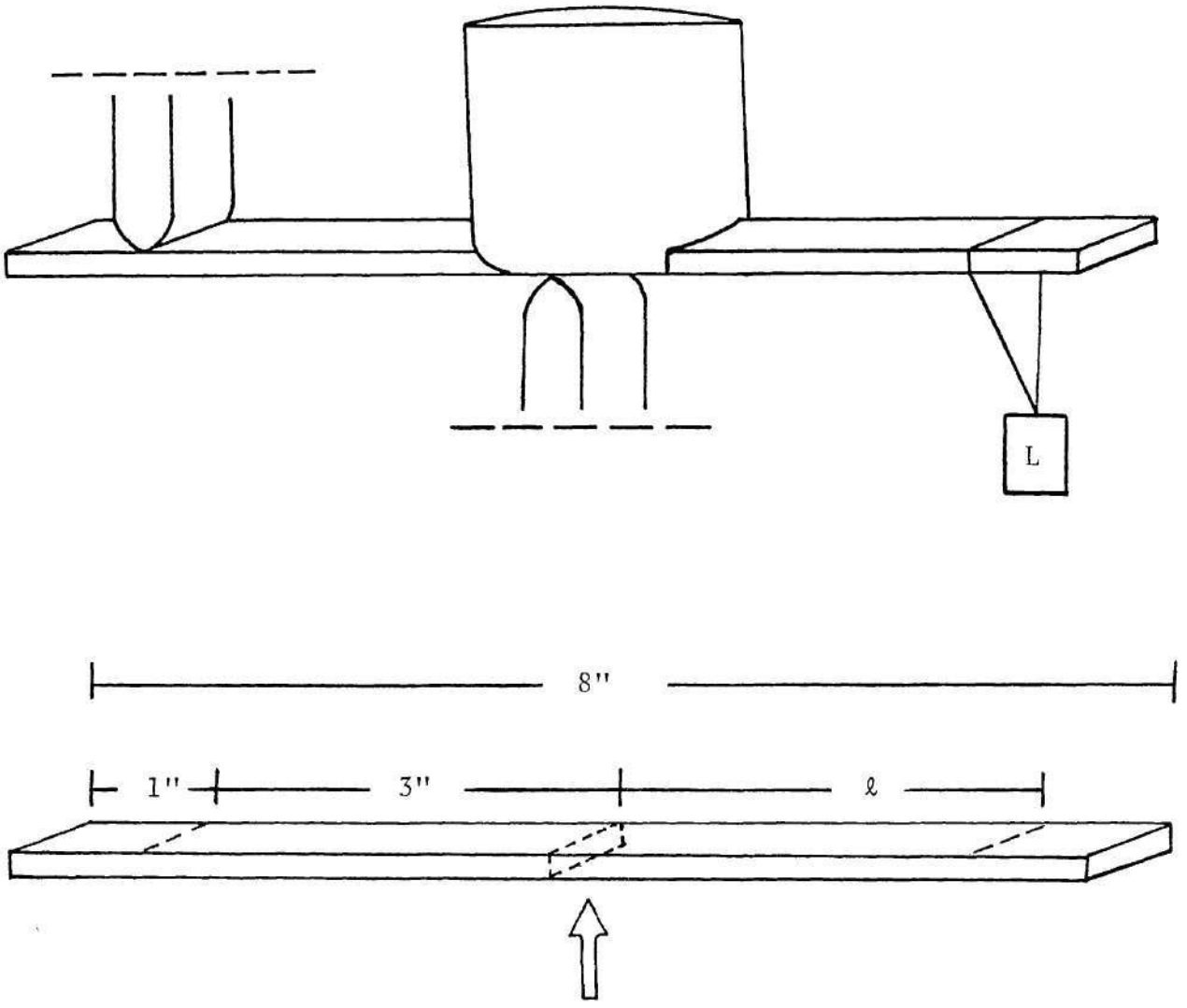

Figure 3. Schematic Diagram of the Apparatus Showing the Specimen Loading Location and the Critical Dimensions

The apparatus used for testing the specimens was constructed specifically for this work. The system allowed six specimens to be tested at the same time. The two horizontal bars were machined to accurate dimensions in the areas where the specimens were tested. In such a way the stress applied in the specimen could be calculated. The detailed calculations are contained in Appendix A.

The application of stress was obtained by hanging the load at the free end of the specimen as shown in Figure 3. The maximum stress occurs at the support in the middle of the specimen. This area of maximum stress was immersed in the corrosive solution by using a plastic cup, cut at the bottom and attached to the specimen with silastic for a water tight seal.

To achieve the application of voltage a cathode was immersed in the solution and a battery was used to achieve the desired potential differences. The cathodes were made of pure carbon and of course the specimens were the anodes. With this enlarged cathode a higher corrosion rate could be obtained.

The solution used for all experiments was 3.5 sodium chloride and the pH was 3.0. A 3.0 pH brings the system into the active corrosion area of the Pourbaix diagram as shown in Appendix B. This provides a method for accelerating the tests and obtaining graphitization data in a reasonable period of time.

Specimens

Two different types of cast iron were examined. The first had been exposed in service for several years material (material A) and the second was a new "as cast" material (material B). The composition of both materials after the chemical analysis was made, is presented in Table 1.

Table 1. Composition of the Two Types of the Tested Cast Iron

%	F_e	C	Mn	Si	Ni	Cr	Cu	P	S
Material A	Balance	3.55	.48	1.33	.1	.02	.01	.73	.13
Material B	Balance	3.51	.32	1.62	.55	.16	.44	.26	.11

The microstructure determination showed that the exposed (in service material) has a type B (ASM Handbook) distribution of graphite flakes, characterized by rosete grouping and random orientation. Some interdendritic segregation was found also.

The unexposed material has a type D distribution of graphite flakes, characterized by interdendritic segregation and random orientation. The microstructure of both materials is shown in Figure 4 and Figure 5.

The average tensile strength of material A and B was:

Figure 4. 100X Magnification. Unetched Microstructure of Material A

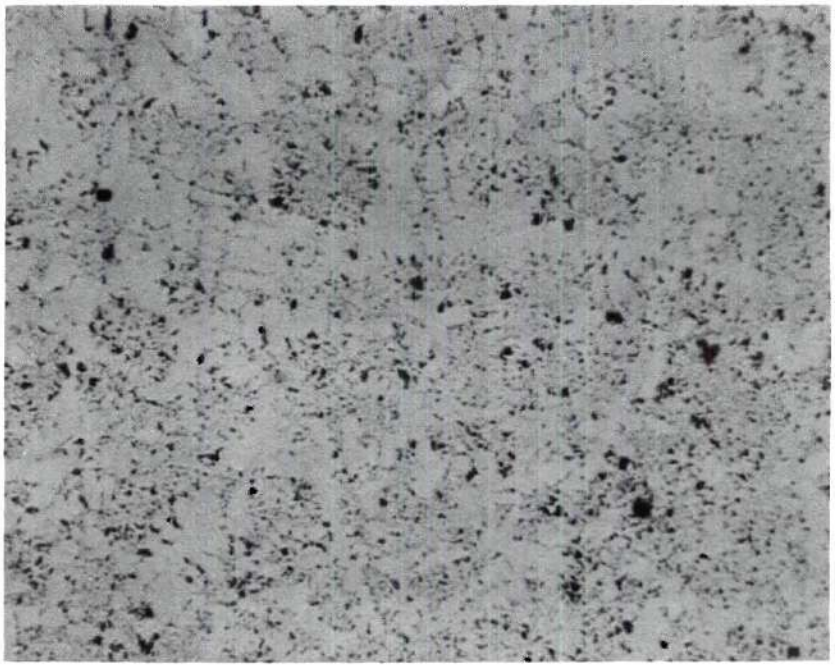

Figure 5. 100X Magnification. Unetched Microstructure of Material B

	Average Tensile Strength
Material A	70,000 psi
Material B	73,000 psi

Small specimens with dimensions about .25" x .5" x 75" were used for the first phase of the experiments and bars about .16" - .25" x .5" x 8" were used for the second and third phase. The residual stresses were produced by heating the specimens locally with a welding torch at elevated temperatures for a period of time. In cast iron there is no way to accurately measure residual stress so this work had to be qualitative.

Experimental Procedure

Initially the specimens were cut to the appropriate dimensions and the residual stresses were induced in the specimens by local torch heating to what was considered similar temperatures each time.

Specimens for the third phase of experiments were machined with an accuracy ± .001 in. This was done to allow the determination of the accurate value of the applied stress in these experiments. Once the specimen was seated in the apparatus the load was hung at the position calculated for the specimen dimensions.

For the application of potential difference a cathodic carbon electrode was immersed in the solution and the carbon electrode and the specimen connected to the battery through a voltmeter. The value of the voltage applied was

0.2 volts per cell and the specimens were connected parallel. Figure 6 shows a schematic diagram of a typical cell. The voltage was applied to raise the electrochemical potential of cast iron, increase the corrosion current and to accelerate the test. The initial condition without applied potential and the final state after the voltage has been applied is shown in Figure 7.

The specimens after set periods of time (for the first phase), or after they broke (for the second and third phase), they were removed from the test sites, cleaned and prepared for metallographic examination. The average and maximum depth of pits were then recorded to evaluate the extent of corrosion on the specimens. Tables 2, 3, and 4 outline the analysis and conditions of the first, second and third phase experiments.

Potentiostatic Measurements

Potentiostatic and corrosion current measurements were made in order to investigate the electrochemical properties of materials A and B and compare their corrosion behavior.

A Keithley, 602 solid state electrometer was used for the determination of the corrosion potential and the change of the corrosion potential and corrosion current with the time of various galvanic couples is given in Table 5.

The 1070 steel was selected because its composition

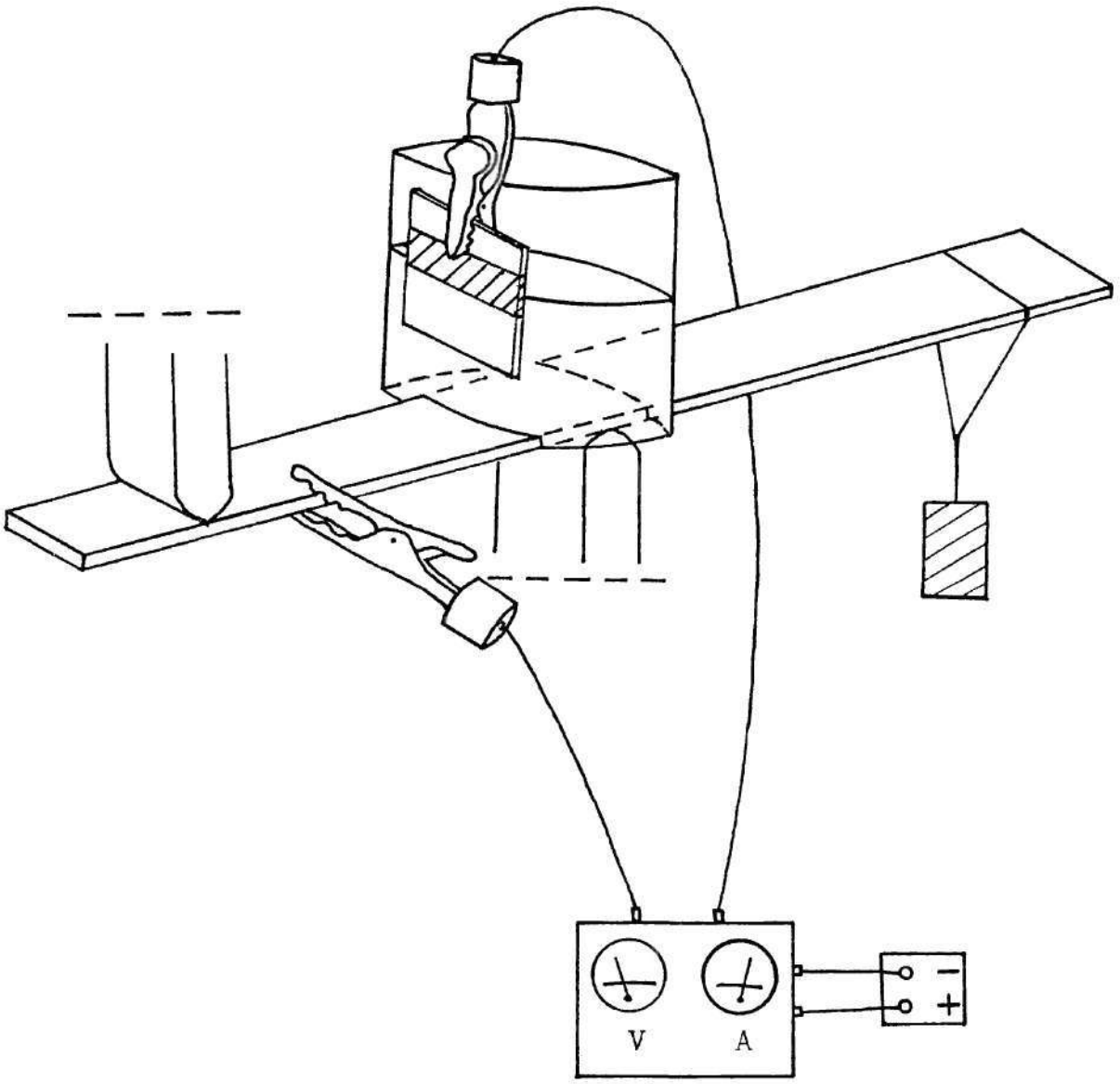

Figure 6. The Arrangement of the Specimen, Cup, Graphite Cathode and Battery During the Application of an External Potential

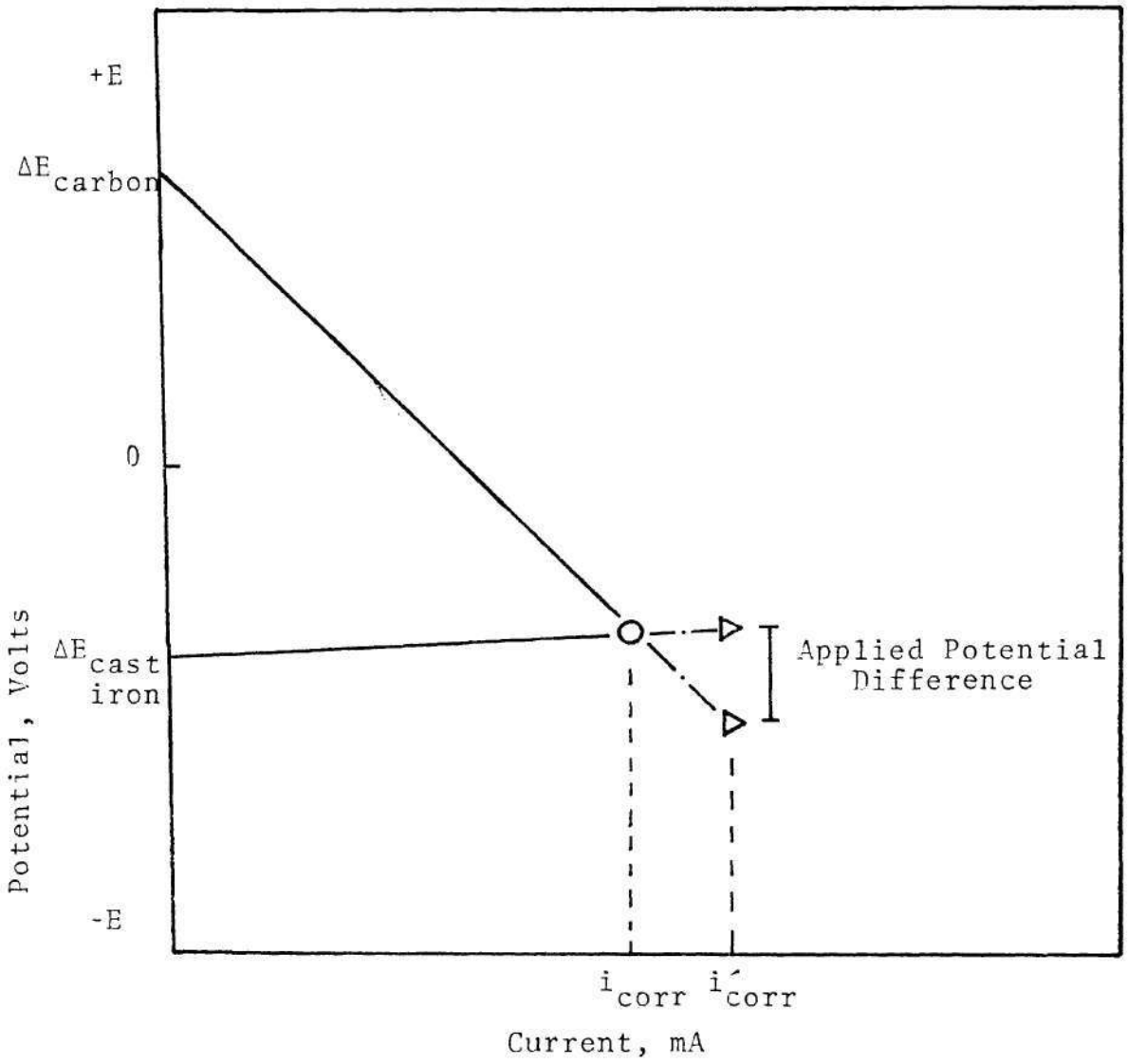

Figure 7. A Polarization Diagram Representation of Initial (1) and Final (2) Conditions for Voltage Application

Table 2. Phase I Experimental Conditions. The four cases cited have been performed for both A and B materials.

PHASE I

Case I	Case II	Case III	Case IV
1. No Stress	1. No Stress	1. No Stress	1. No Stress
2. No Current	2. No Current	2. Current	2. Current
3. No Residual Stresses	3. Residual Stress	3. No Residual Stresses	3. Residual Stress
4. Corrosive Solution	4. Corrosive Solution	4. Corrosive Solution	4. Corrosive Solution

Table 3. Phase II Experimental Conditions. The four cases cited have been performed for both A and B materials.

PHASE II

Case I	Case II	Case III	Case IV
1. Stress	1. Stress	1. Stress	1. Stress
2. Solution	2. Solution	2. Solution	2. Solution
3. Current	3. Current	3. No Current	3. No Current
4. Residual Stresses	4. No Residual Stresses	4. No Residual Stresses	4. Residual Stresses

Table 4. Phase III Experimental Conditions. The four cases cited have been performed for both A and B materials.

PHASE III

Case I	1. Solution 2. Stress, σ = 40,000 psi 3. Current, (v = 0.2 volts)
Case II	1. Solution 2. Stress, σ = 40,000 psi 3. No Current
Case III	1. Solution 2. Stress, σ = 55,000 psi 3. Current, (v = 0.2 volts)
Case IV	1. Solution 2. Stress, σ = 55,000 psi 3. No Current
Case V	1. Solution 2. Stress, σ = 65,000 psi 3. Current, (v = 0.2 volts)
Case VI	1. Solution 2. Stress, σ = 65,000 psi 3. No Current

Table 5. Galvanic Couples Tested. Corroded cast iron 1 = corroded cast iron only on the surface; corroded cast iron 2 = corroded cast iron with graphitic layer

Couple I	Couple II	Couple III	Couple IV	Couple V
1070 Steel	Material A	Material B	Material A	Material B
and	and	and	and	and
			A. Corroded Cast Iron 1	A. Corroded Cast Iron 1
Pure Carbon (graphite)	Pure Carbon	Pure Carbon	B. Corroded Cast Iron 2	B. Corroded Cast Iron 2

is similar to the matrix of materials A and B. The reference electrode was a saturated calomel electrode, and the arrangement of the electrodes and equipment is shown in Figure 8. The stabilization time for the potential difference measurements was two and a half hours, and the variation of corrosion potential and corrosion current was observed for four hours.

a.

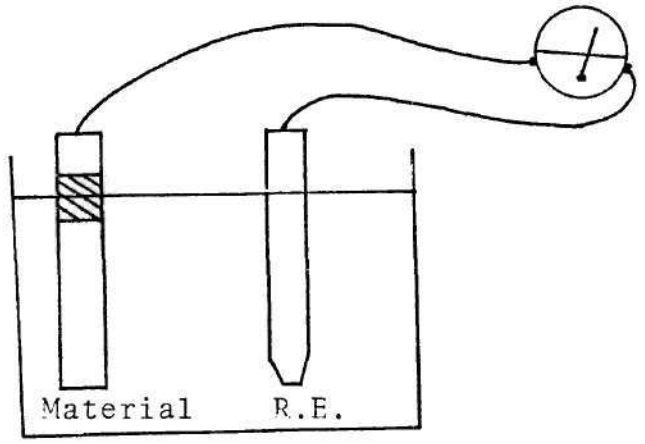

b.

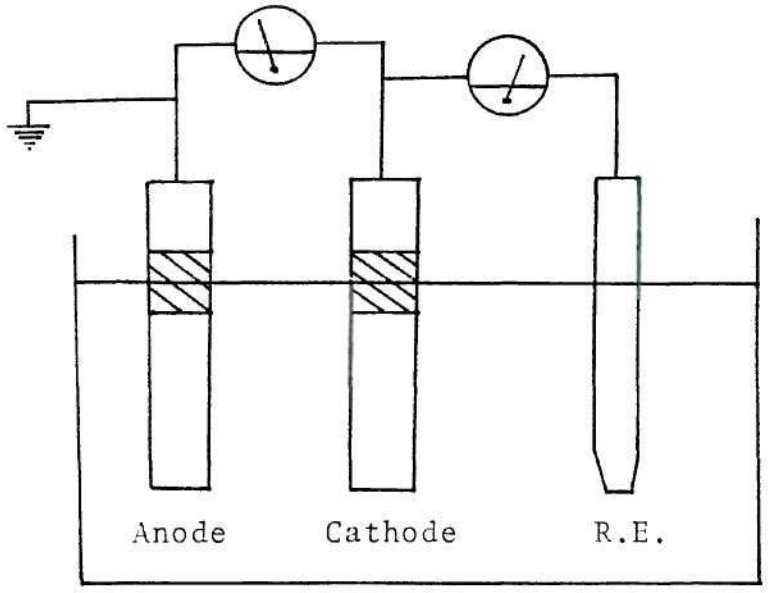

Figure 8. Schematic Drawing of the Cells
(a) Cell for the Potential Difference Measurements
(b) Cell for the Detection of the Variation in Corrosion Potential and Current Versus Time

CHAPTER IV

RESULTS AND DISCUSSION OF RESULTS

Polarization Measurements

The open circuit potentials and the corrosion potentials and currents for the five galvanic couples as measured in a 3.5 percent sodium chloride solution are presented in Table 6. The electrochemical potentials of steel and materials A and B were about the same. The graphite layer exhibited a potential several hundred millivolts more noble than the nongraphitized cast iron or 1070 steel reversifying its cathodic behavior relative to the underlying matrix as reported in the literature.

Figure 9 and 10 show the variation of the potential and current for the five galvanic couples as a function of time, the corrosion potential and current were obtained and using the open circuit potentials, Figure 11 was plotted, assuming linear cathodic and anodic reactions. It shows that the corrosion current of both materials A and B is higher than that of steel. The cells IVa and Va (cast iron against the corroded surface of cast iron) showed a lower corrosion rate than steel, but cells IVb, Vb showed a higher corrosion rate than steel. The more noble the cathode (cast iron corroded on the surface, graphite layer, pure carbon)

Table 6. Open Circuit Potentials and Corrosion Potentials and Currents for the Five Galvanic Couples

Couples Number	Potential Difference	Potential & Current of Corrosion
No. I	ΔE_{carbon} = +628 mV ΔE_{steel} = -699 mV	E_{corr} = -550 mV i_{corr} = 30 mA
No. II	ΔE_{carbon} = +628 mV $\Delta E_{mat\ A}$ = -700 mV	E_{corr} = -642 mV i_{corr} = 35 mA
No. III	ΔE_{carbon} = +628 mV $\Delta E_{mat\ B}$ = -690 mV	E_{corr} = -640 mV i_{corr} = 435 mA
No. IV	$\Delta E_{mat\ A}$ = -700 mV a. ΔE_{cci1} = -668 mV b. ΔE_{cci2} = -308 mV	E_{corr} = -680 mV i_{corr} = 225 mA E_{corr} = -594 mV i_{corr} = 310 mA
No. V	$\Delta E_{mat\ B}$ = -690 mV a. ΔE_{cci1} = -655 mV b. ΔE_{cci2} = -310 mV	E_{corr} = -662 mV i_{corr} = 24 mA E_{corr} = -646 mV i_{corr} = 325 mA

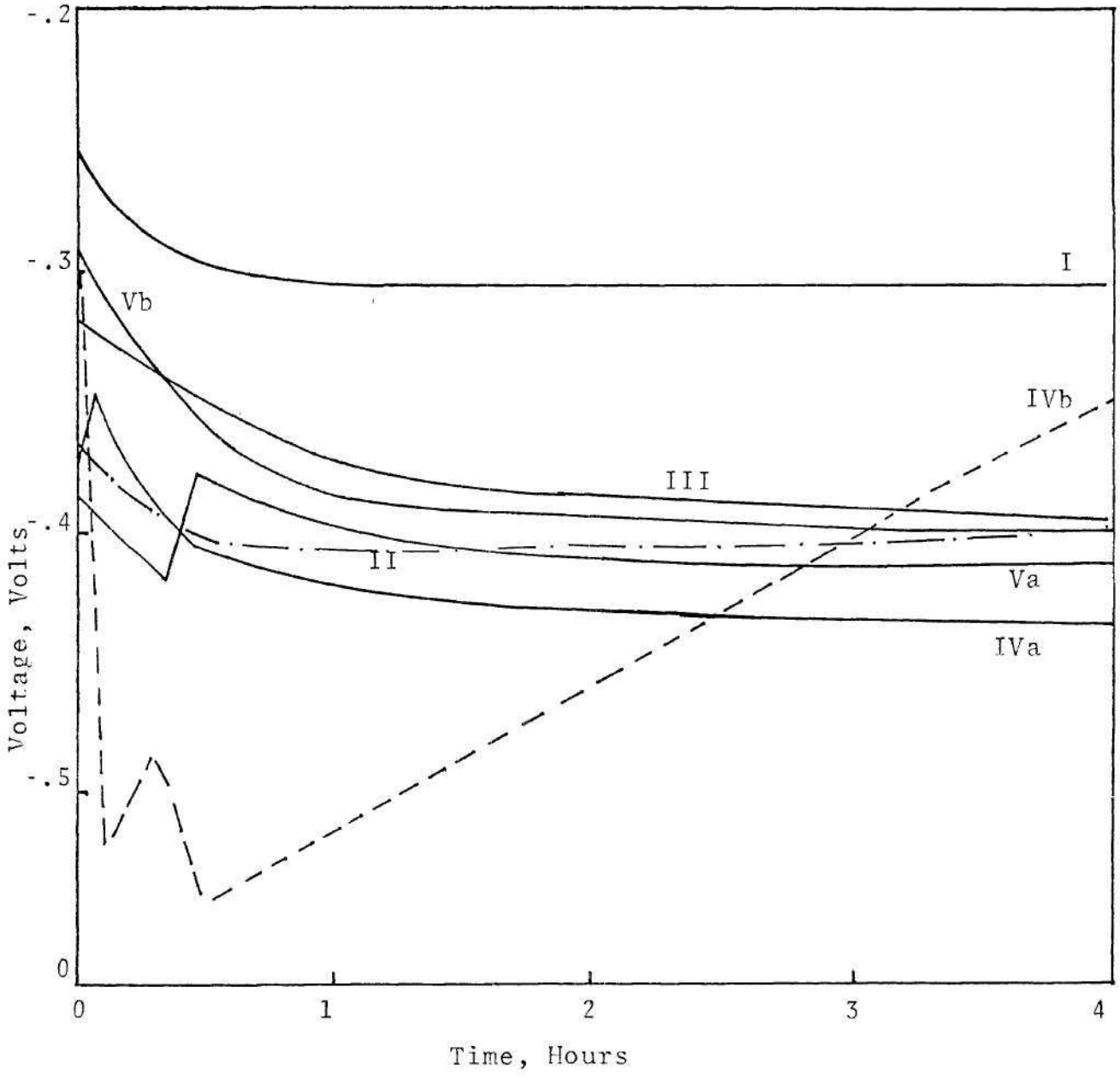

Figure 9. Corrosion Potential as a Function of Time for the Five Galvanic Couples

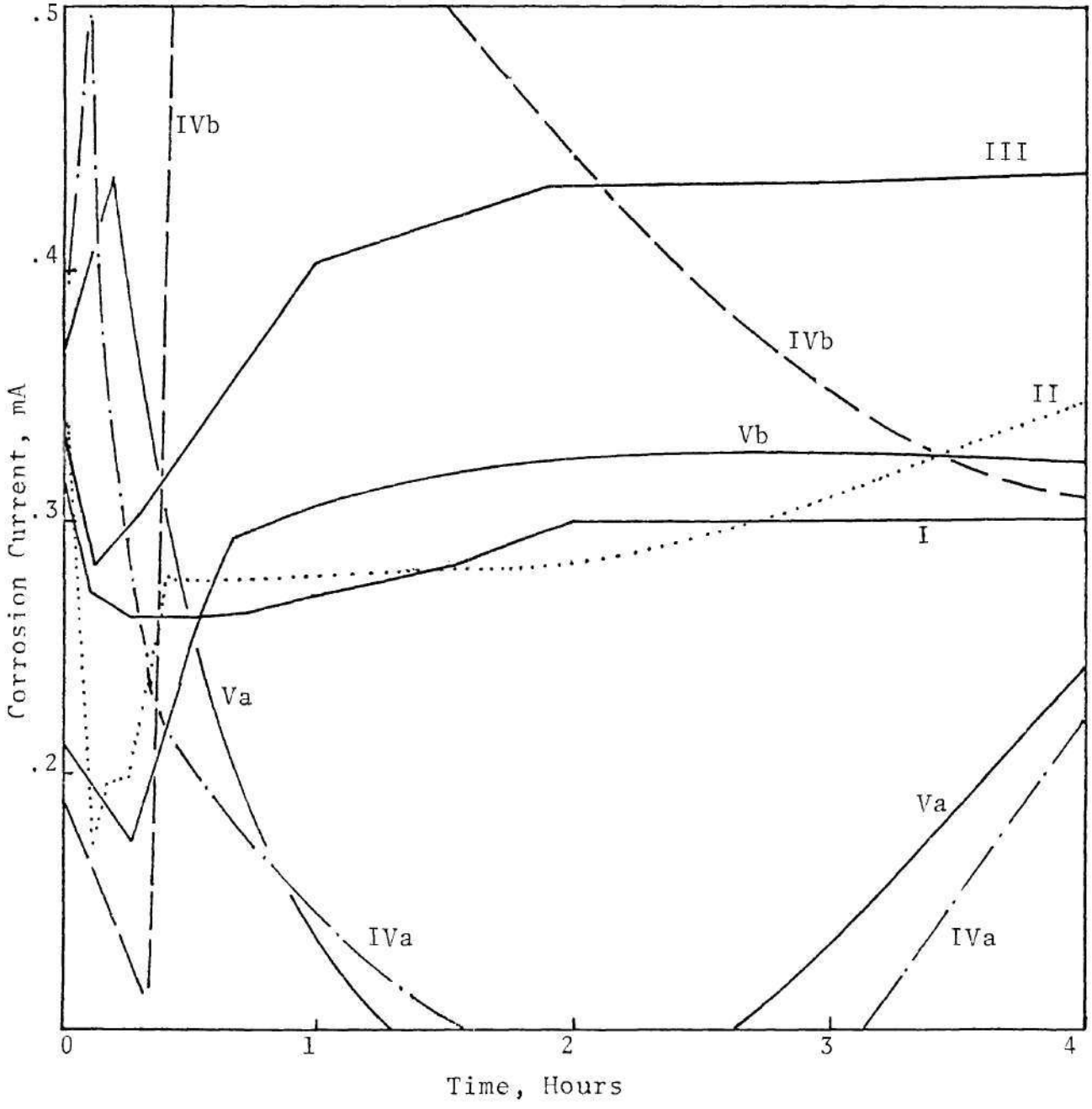

Figure 10. Corrosion Currents as a Function of Time for the Five Galvanic Couples

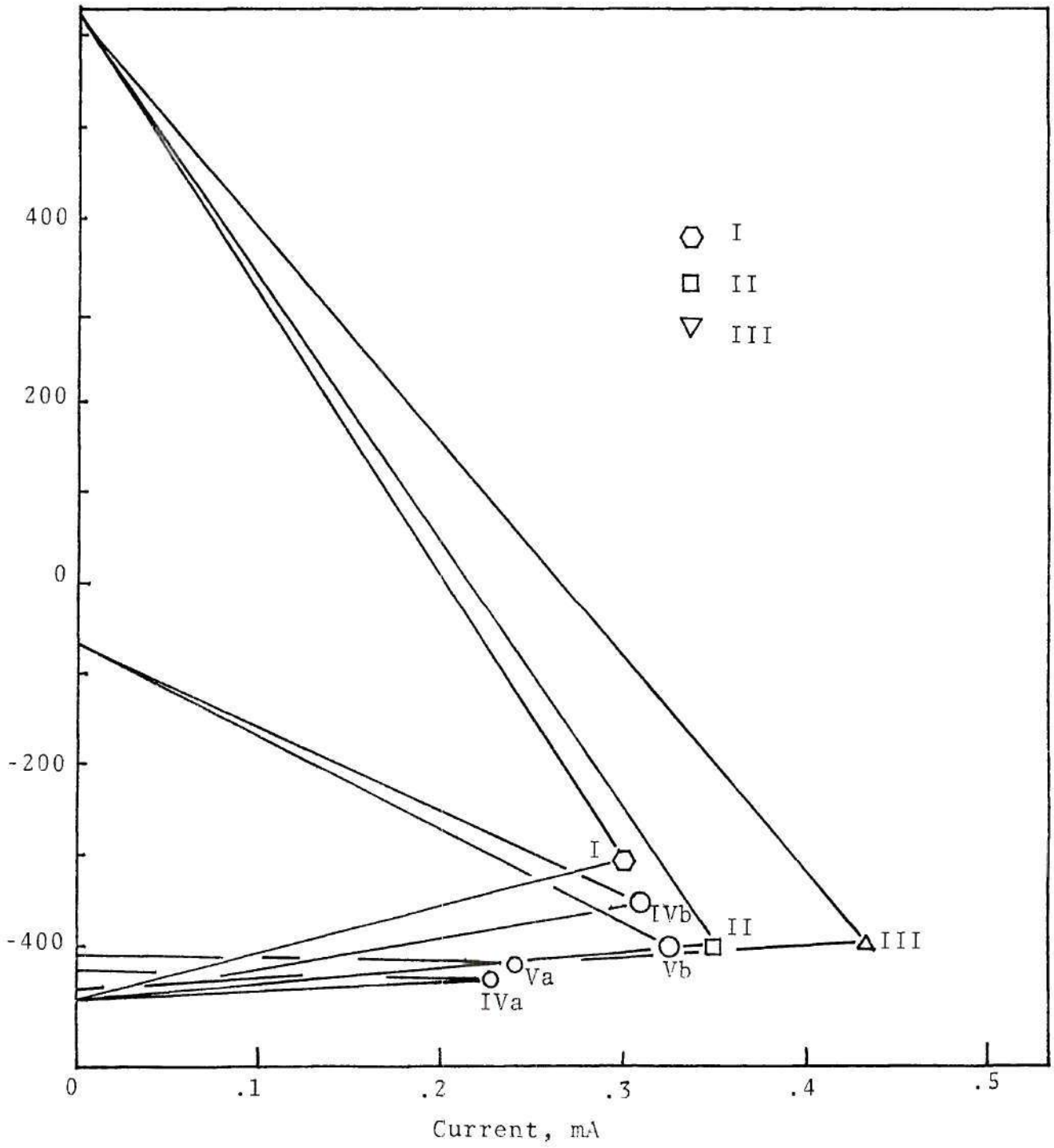

Figure 11. Combined Activation Polarization Curves for the Five Galvanic Couples

the higher is the graphitic corrosion current. In other words, as the graphitic corrosion proceeds from non-corroded cast iron to corroded on the surface and later forming the porous graphite layer on the surface, the graphitic corrosion current increases according to the increase of the nobility of the cathode.

Graphitic Corrosion Measurements

Table 7 gives the exposure time, maximum and average penetration and maximum and average corrosion penetration rates, plus the averages for each experiment in phase I and for both materials A and B.

The average penetration in the absence of current was zero in case I and case II. However a measurable maximum penetration was found though both were small case II attack for heat induced was greater than for case I. With applied voltage (case III and case IV) the maximum and average penetration showed marked increases. The maximum and average penetration rates of case IV are higher than those of case III. The greatest difference was in the maximum corrosion rate which increased 1.5 times the average corrosion rate. This can be related to the effect of residual stress in the specimens of case IV. Materials A and B corroded at about the same rate except the maximum corrosion rate for material A from case III to case IV, was greater than for material B. The residual stresses generally increased the corrosion rate,

Table 7. Exposure Time, Maximum and Average Penetration and Penetration Rate for Phase I Experiments, for Materials A and Material B

Case	Exposure Time (Days)		Penetration (inches$\times 10^2$)				Penetration Rate (in$\times 10^2$/day)			
			Maximum		Average		Maximum		Average	
	A	B	A	B	A	B	A	B	A	B
No.I	103	99	.20	.15	0	0	.0019	.0015	0	0
Average	101		.175		0		.0017		0	
No.II	110	102	.40	.70	0	0	.0036	.0068	0	0
Average	106		.55		0		.0052		0	
No.III	102	104	16	16	14	14.8	.156	.154	.138	.142
Average	103		16		14.4		.155		.140	
No.IV	66	104	16	15	13	14.2	.240	.144	.197	.136
Average	85		15.5		13.6		.193		.166	

particularly the maximum corrosion rate. This effect was more pronounced when residual stresses were coupled with an applied potential.

Table 8 gives the time to failure under static load, the maximum and average graphitization penetration and the penetration rates at fracture for specimens tested according in phase II. The time to failure in bending increased from case I, to case II, to case IV, to case III. The longer time to failure of case II compared to I, III, and IV may be related to the combined effect of residual stress on the strength of the material and the graphitic corrosion. The decrease in time to failure between case II and I and between III and IV is about a factor of four showing the severe effect of residual stress combined with impressed current.

Figures 12 through 19 present the variation of maximum and average penetration versus time for the four types of phase II experiments. These results showed an increase in maximum penetration and average corrosion attack following the same order as for the time to failure, i.e., case I: case II: case IV: case III.

Figures 20 through 27 present the variation of the maximum and average corrosion rates for the four types of specimens in phase II experiments. These rates again follow the same order, Case I: case II: case IV: case III. However, the maximum corrosion attack rate for case I and case II remains essentially constant for material A. The average

Table 8. Exposure Times (Times to Failure), Maximum and Average Penetration and Penetration Rates for Phase II Experiments, for Material A and Material B

Case	Exposure Time (Days)		Penetration (Inches$\times 10^2$)				Penetration Rate (in$\times 10^2$/day)			
			Maximum		Average		Maximum		Average	
	A	B	A	B	A	B	A	B	A	B
No.I	16.6	14	8.91	10.55	4.17	7	.54	.75	.251	.5
Average	15.3		9.73		5.58		.65		.37	
No.II	41.25	12.8	18.5	9.47	10.25	4.16	.46	.74	.25	.32
AAverage	27		14		7.2		.60		.29	
No.III	39	62	3.5	5	1.5	1.8	.09	.08	.04	.03
Average	50.5		4.25		1.65		.085		.035	
No.IV	38	57	4.5	5	1.55	1.8	.12	.09	.041	.032
Average	47.5		14.75		1.67		.105		.037	

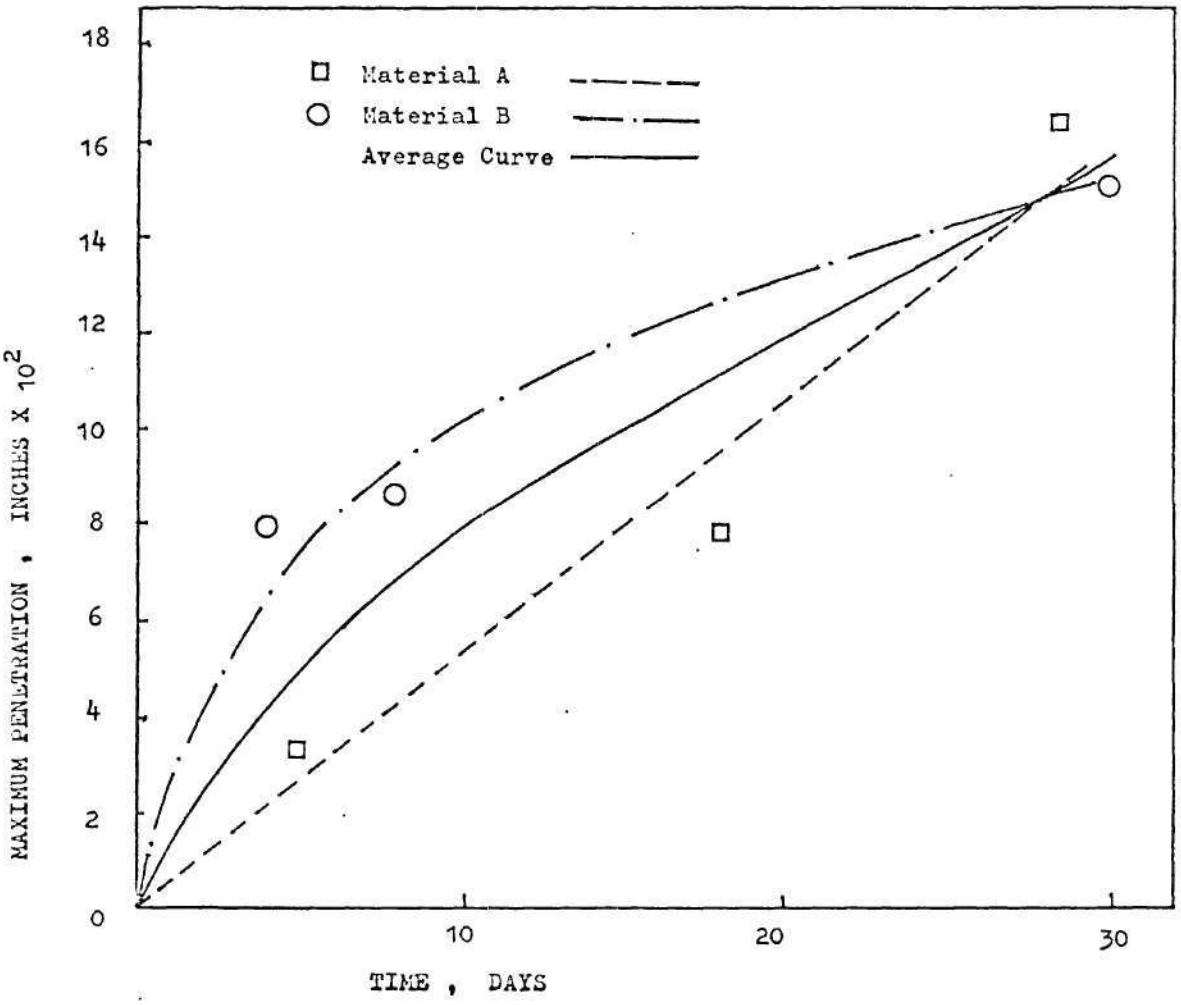

Figure 12. Maximum Penetration Versus Time for Case I of Phase II

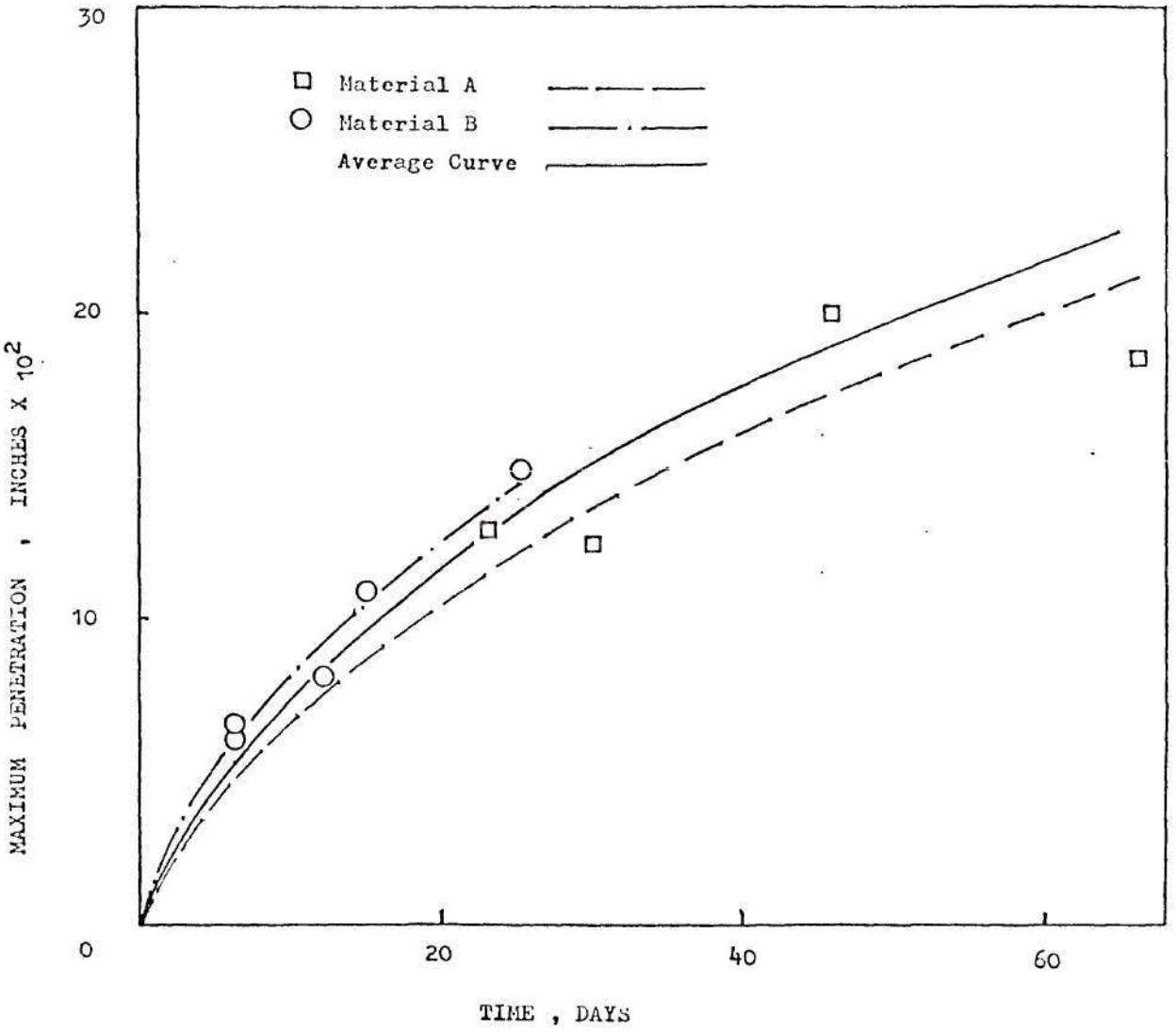

Figure 13. Maximum Penetration Versus Time for Case II of Phase II

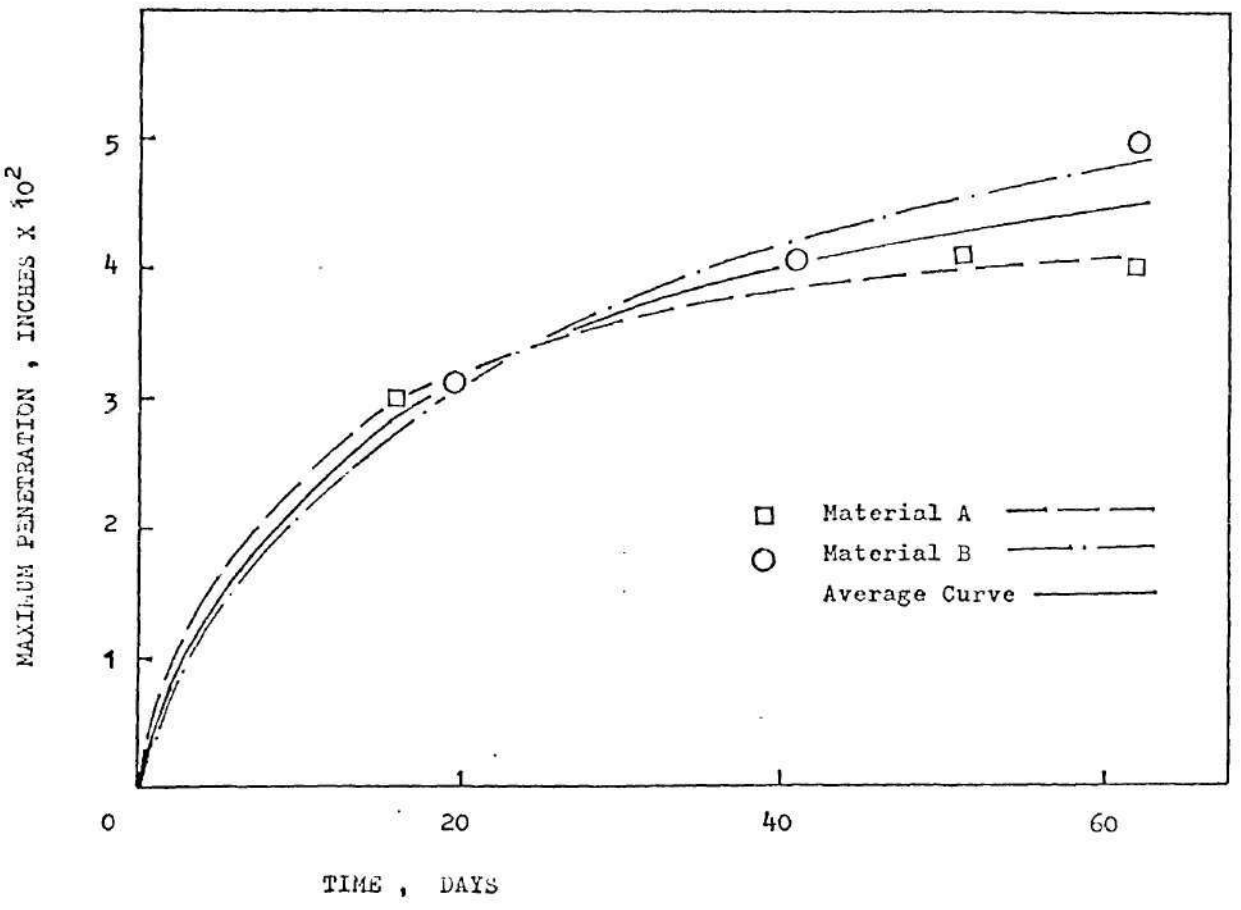

Figure 14. Maximum Penetration Versus Time for Case III of Phase II

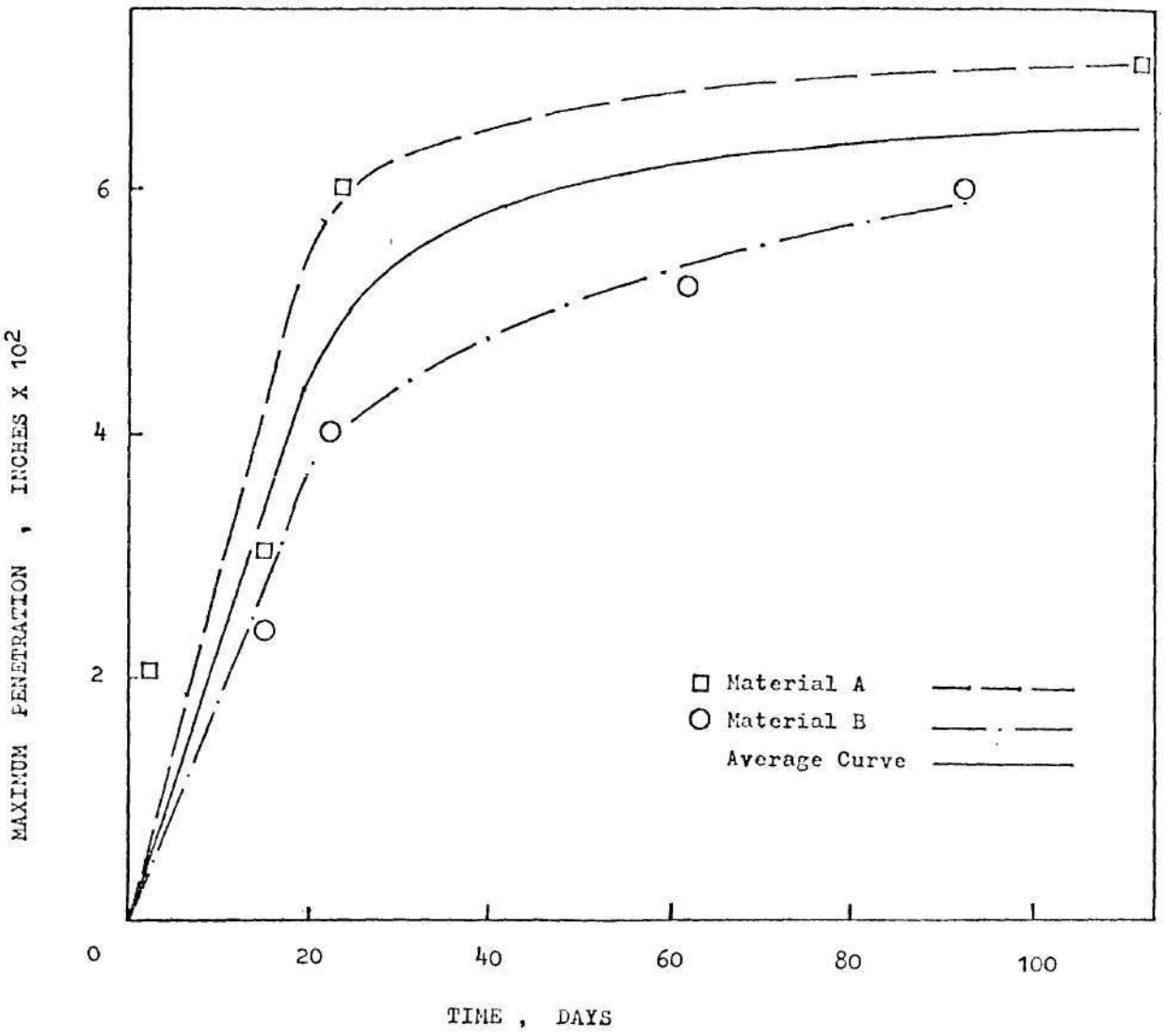

Figure 15. Maximum Penetration Versus Time for Case IV of Phase II

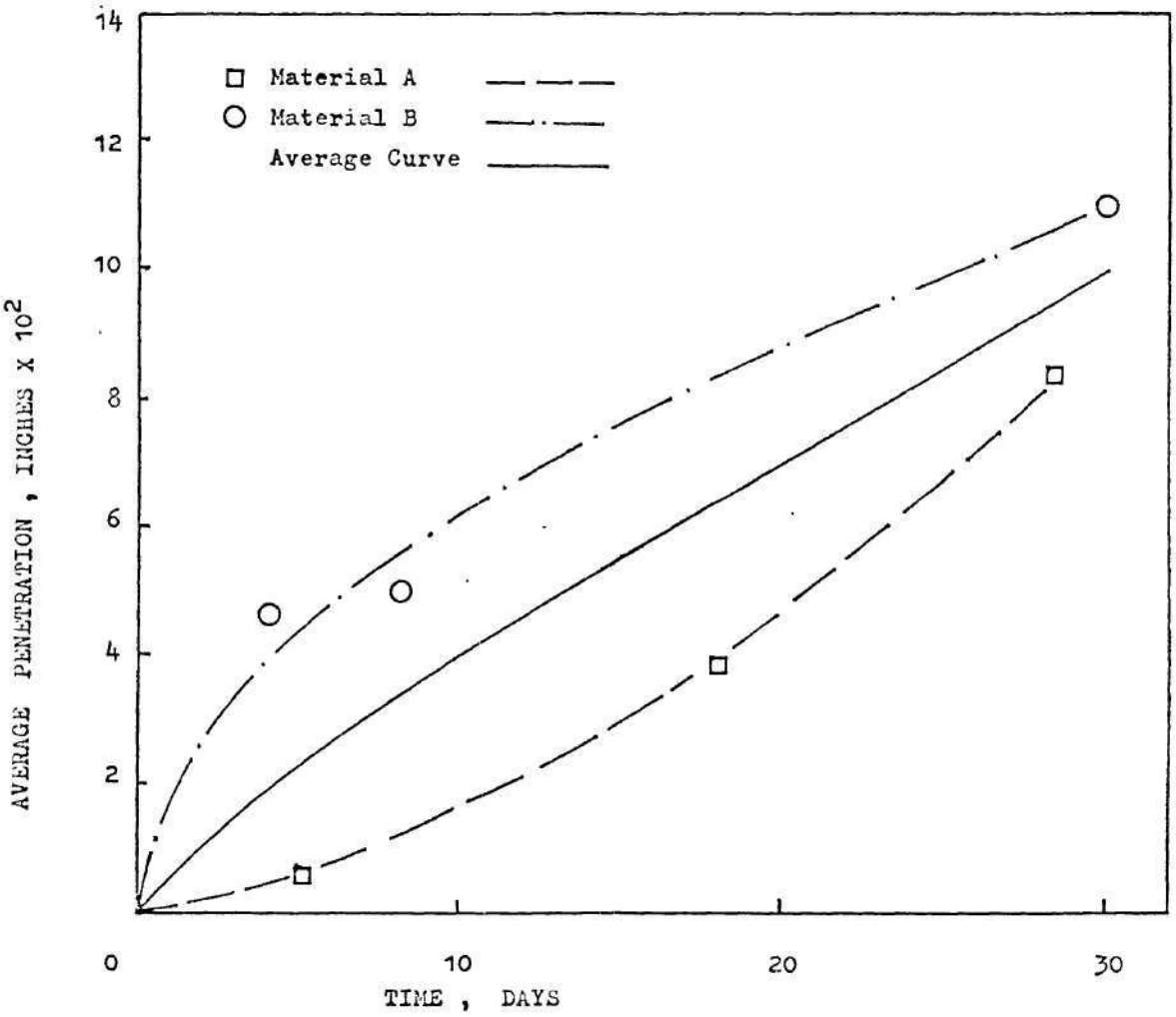

Figure 16. Average Penetration Versus Time for Case I of Phase II

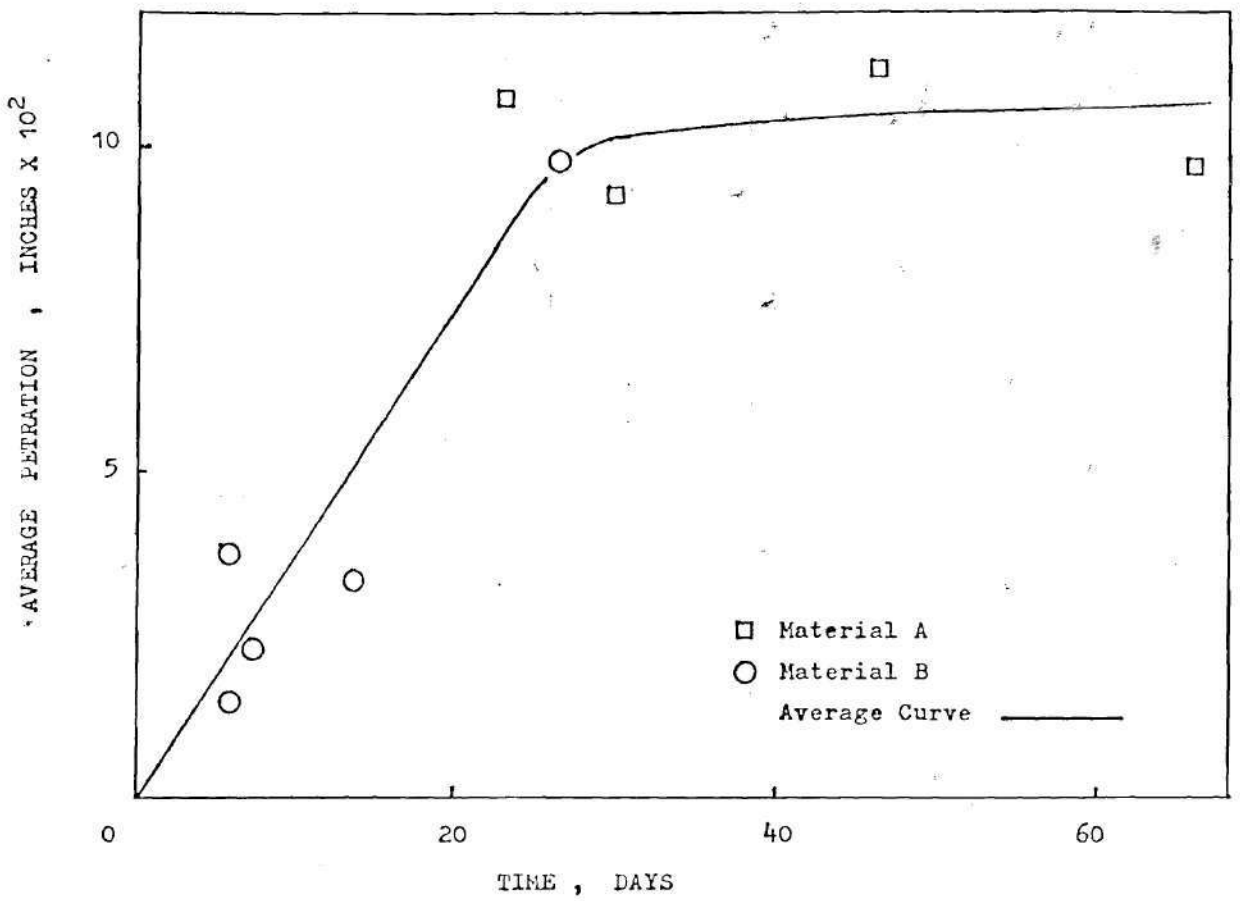

Figure 17. Average Penetration Versus Time for Case II of Phase II

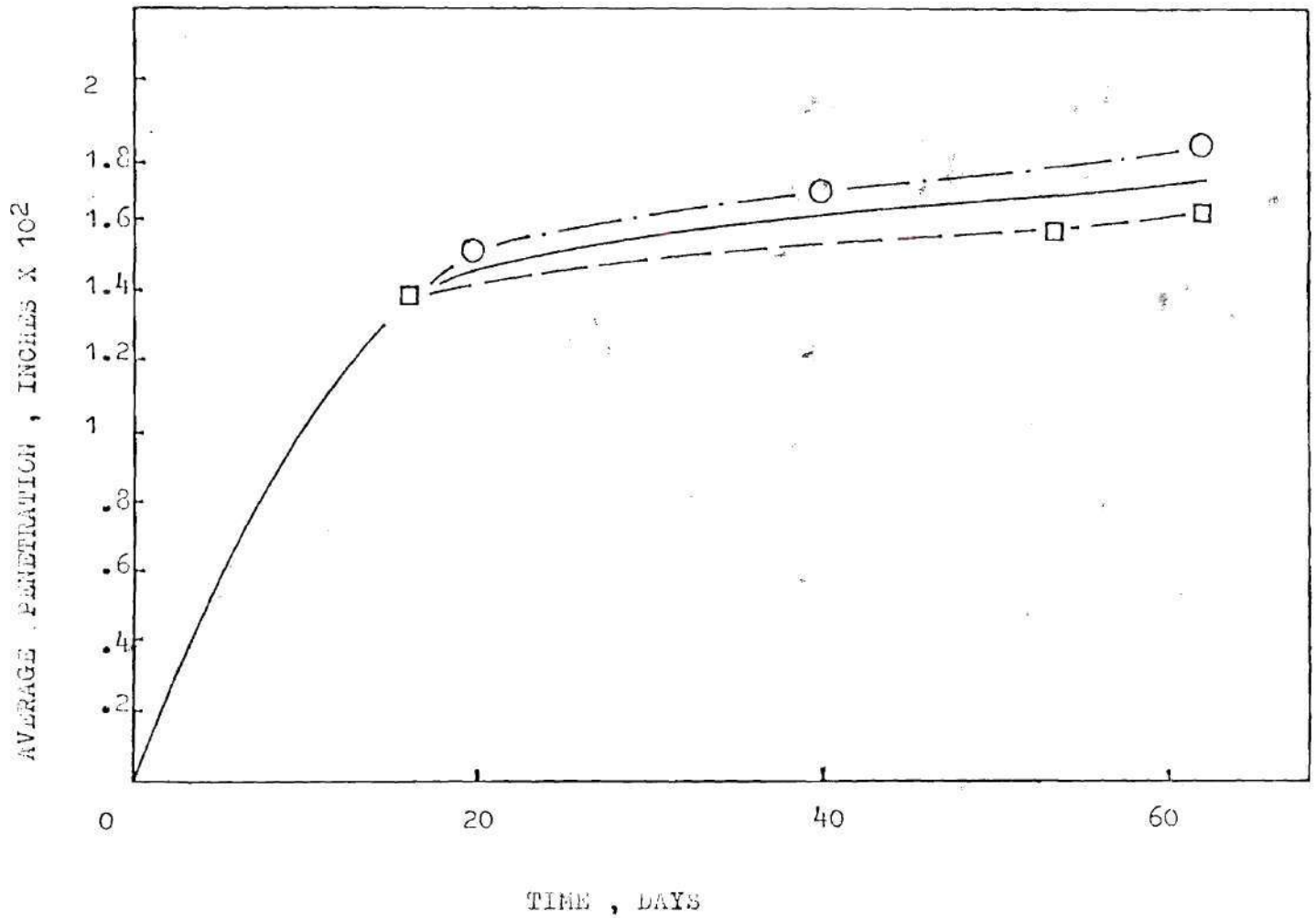

Figure 18. Average Penetration Versus Time for Case III of Phase II

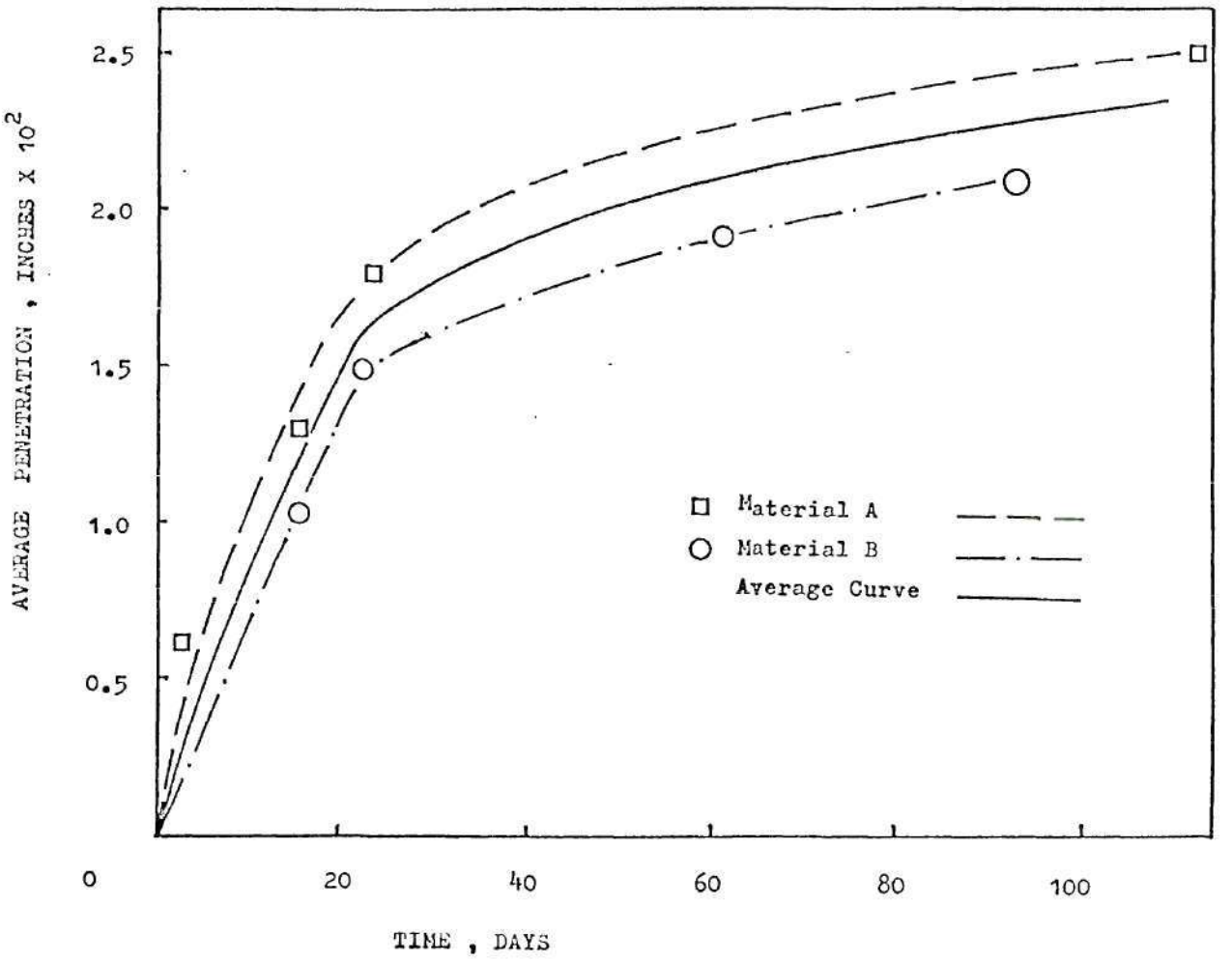

Figure 19. Average Penetration Versus Time for Case IV of Phase II

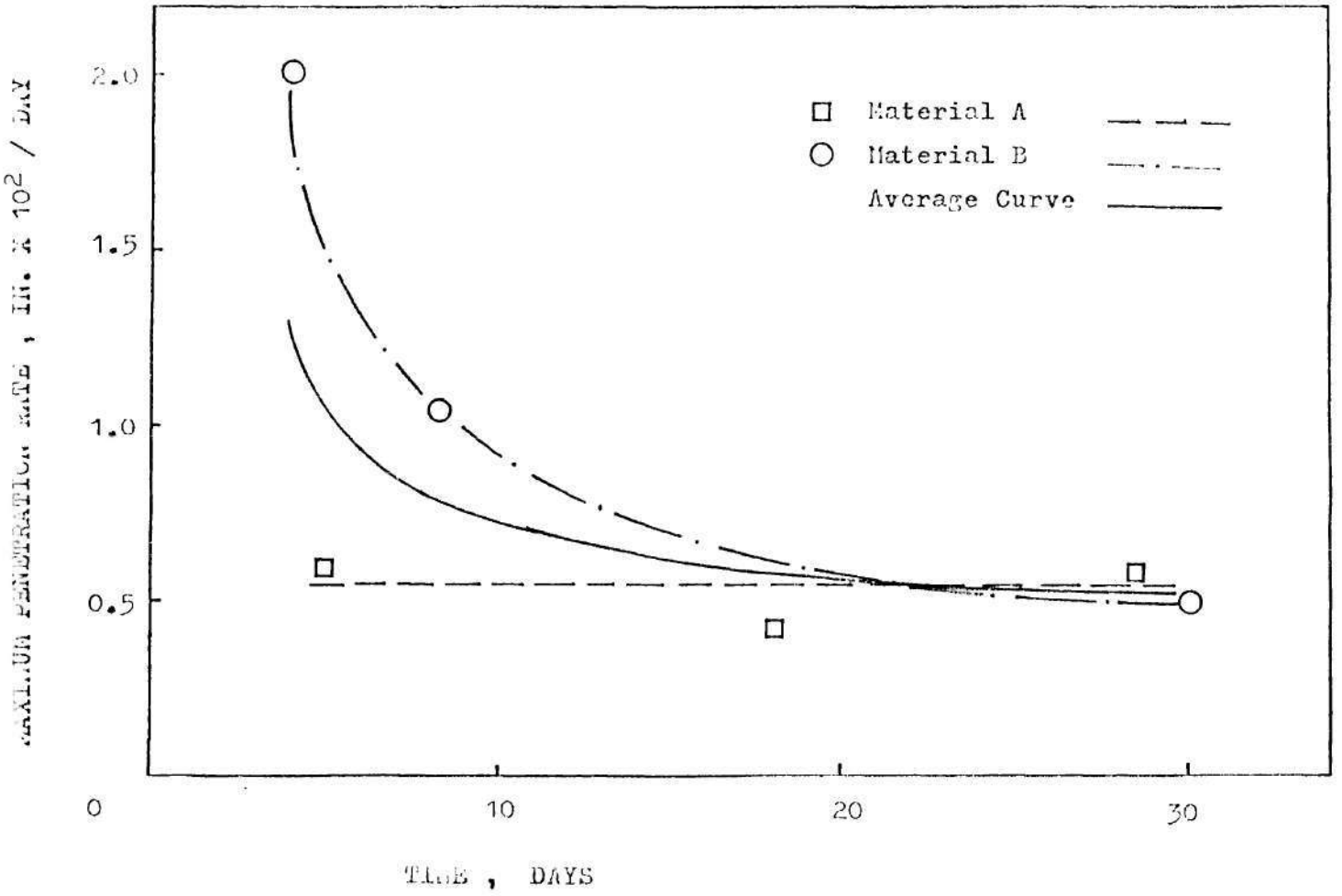

Figure 20. Maximum Penetration Rate Versus Time for Case I of Phase II

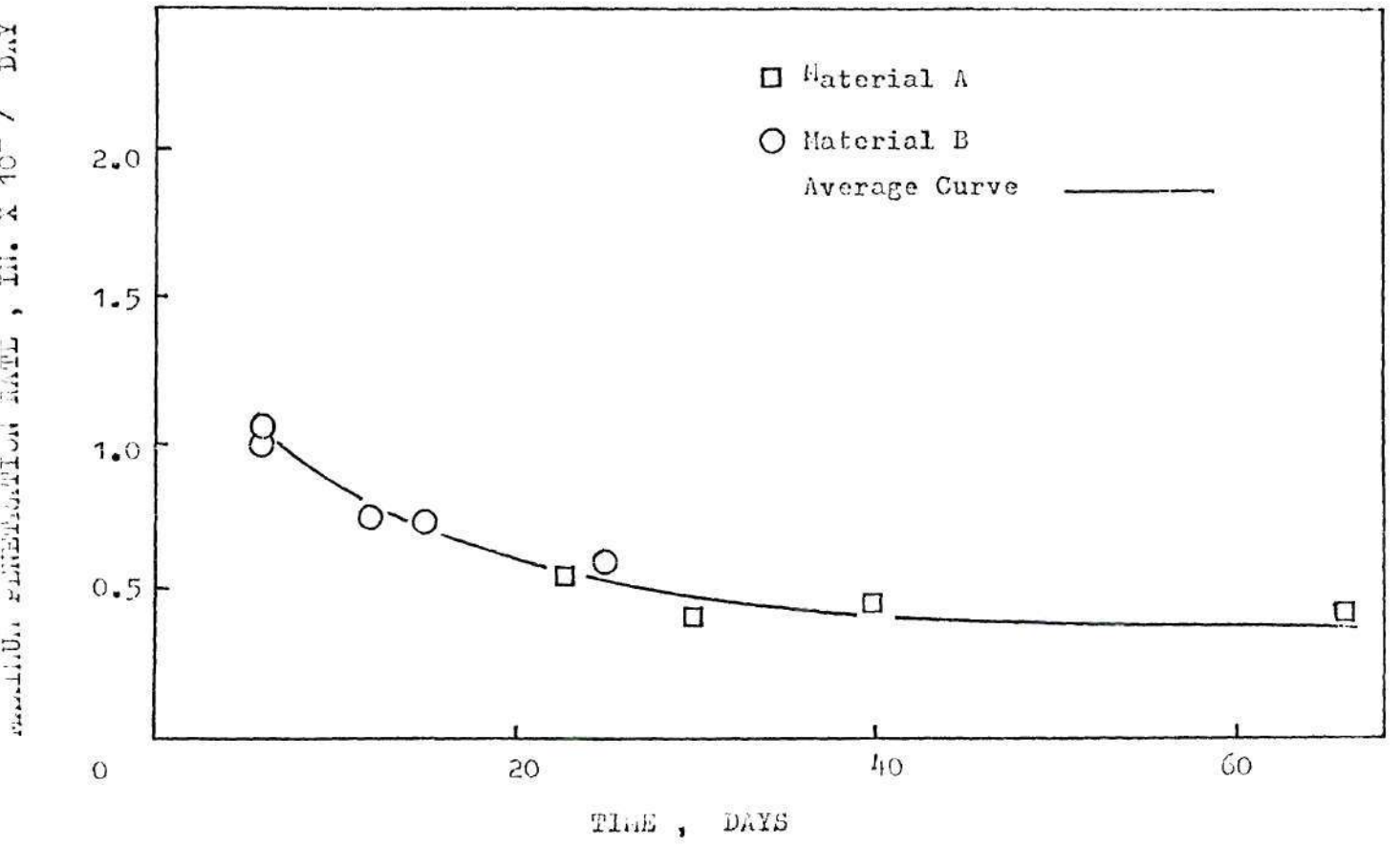

Figure 21. Maximum Penetration Rate Versus Time for Case II of Phase II

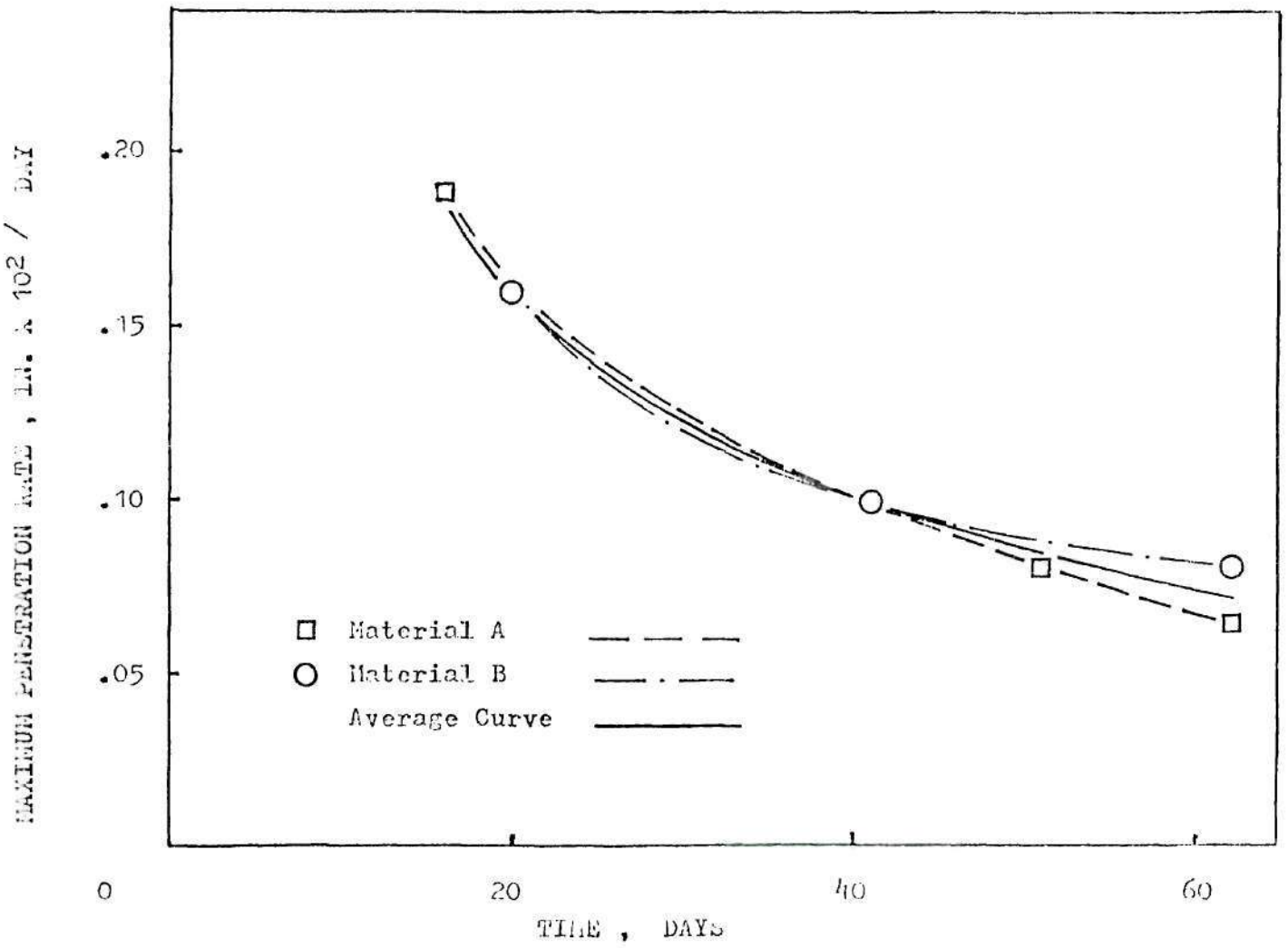

Figure 22. Maximum Penetration Rate Versus Time for Case III of Phase II

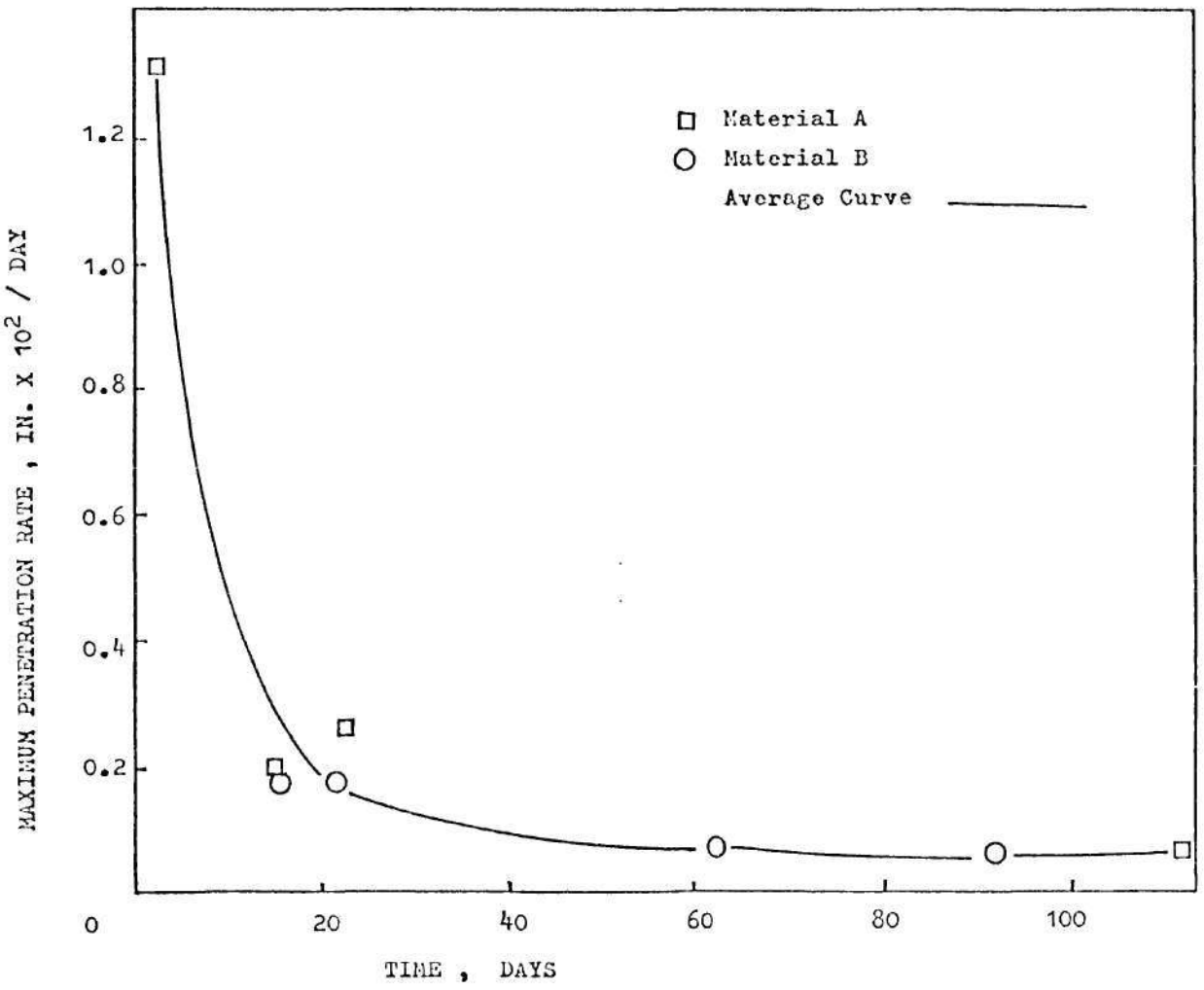

Figure 23. Maximum Penetration Rate Versus Time for Case IV of Phase II

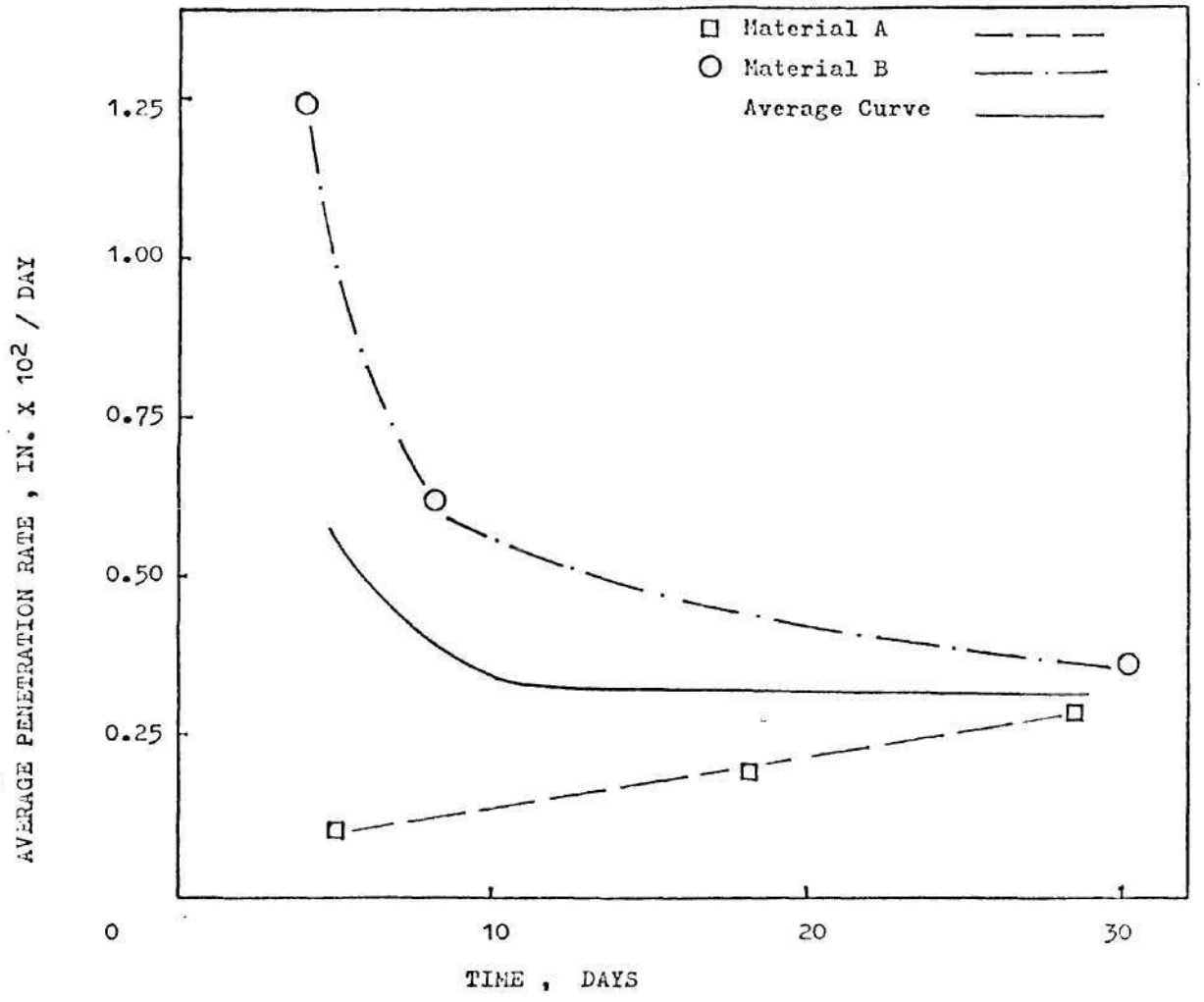

Figure 21. Average Penetration Rate Versus Time for Case I of Phase II

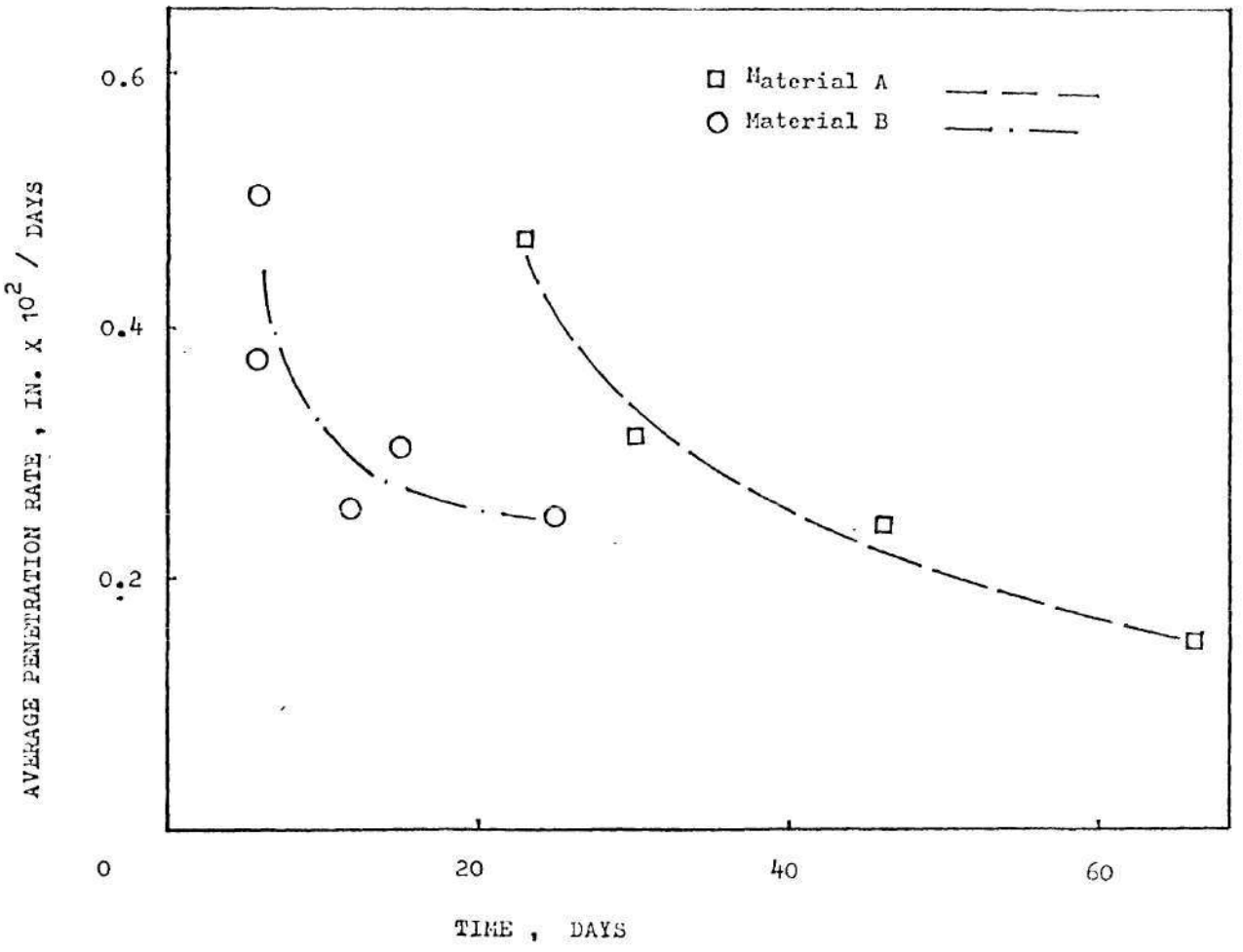

Figure 25. Average Penetration Rate Versus Time for Case II of Phase II

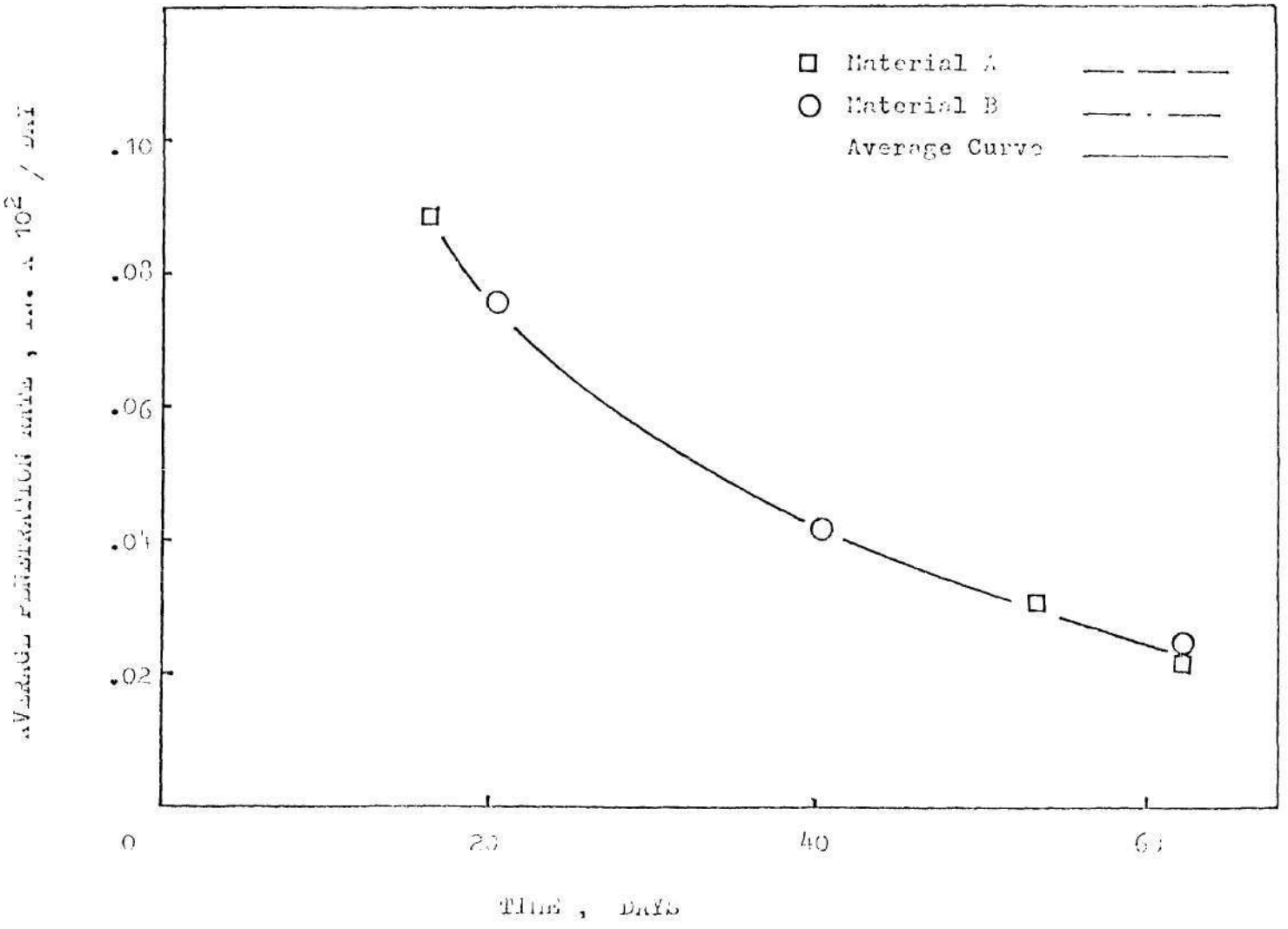

Figure 26. Average Penetration Rate Versus Time for Case III of Phase II

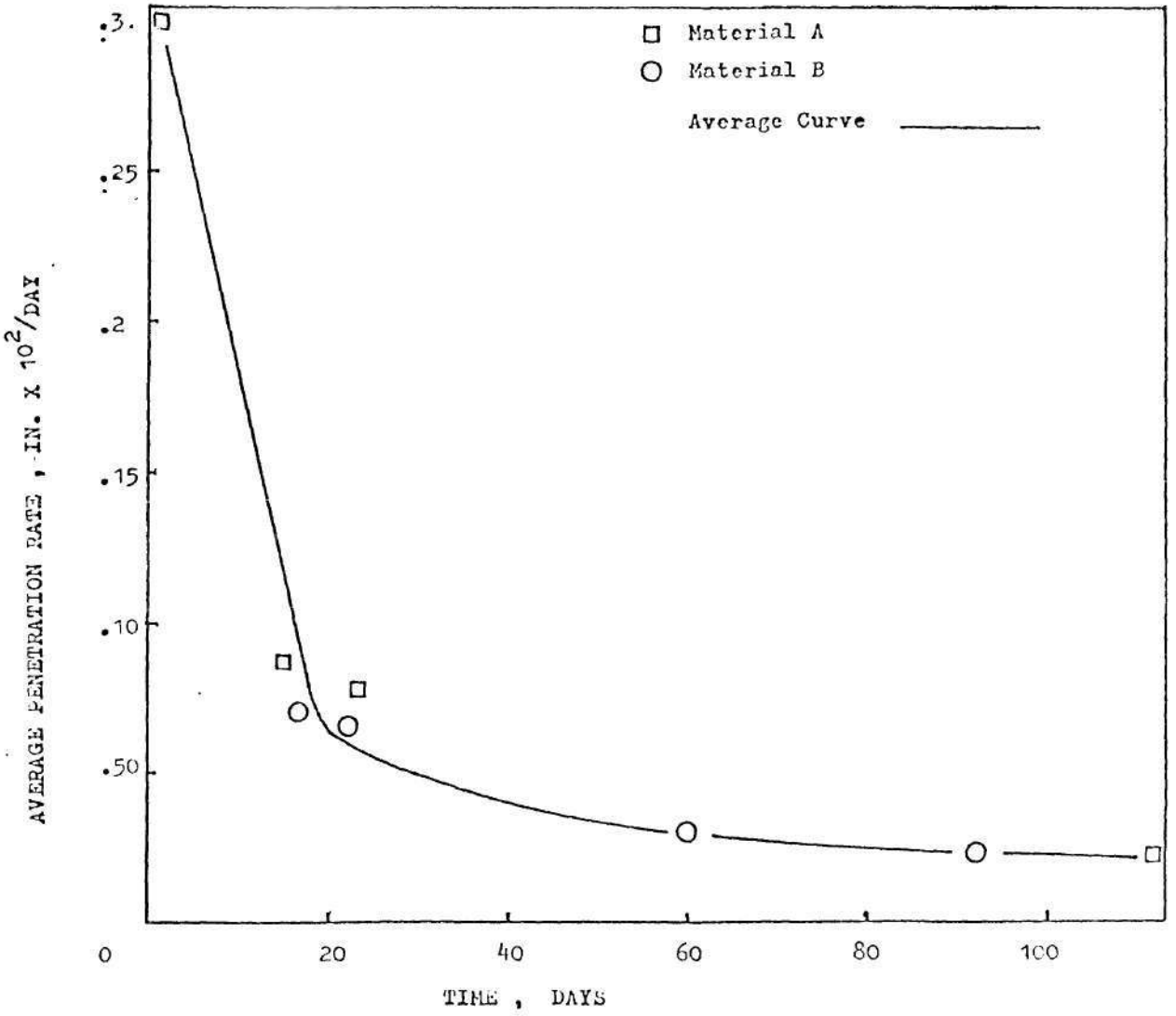

Figure 27. Average Penetration Rate Versus Time for Case IV of Phase II

corrosion rate for the same material in case I had been accelerated, showing that material A is somewhat more sensitive to graphitic corrosion under the combined effects of static load, applied potential and residual stresses.

Comparing studies with the same conditions in phase I and phase II, Table 9 shows the ratio of the maximum corrosion attack rates for phase II to phase I experiments.

In order to determine the effect of static load combined with residual stress and electric current on graphitic corrosion, Table 10 was derived from the test results, showing the ratio of maximum corrosion rate for phase II experiments compared to case I of phase I. The latter had no static load, no impressed current, no residual stress and it has been used as a reference representing a base graphitic corrosion condition.

Table 9. Ratio of Maximum Penetration Rates of Phase II to Phase I Experiments

Phase II	Case III	Case IV	Case II	Case I
Phase I	Case I	Case II	Case III	Case IV
Increase in maximum penetration rate	50	20	4	3.5

Table 10. Ratio of the Maximum Corrosion Penetration Rate Between Phase II and Phase I Case I Experiments

Phase II / Phase I	Case I / Case I	Case II / Case I	Case III / Case I	Case IV / Case I
Increase in maximum penetration rate	400	350	50	60

Investigation of the microstructure of the tested specimens showed that the graphite-rich layer has been locally disturbed, allowing the corrosive solution to penetrate to the base metal. Localized breakdowns of the graphitic layer with "finger-like or fissure" penetration and microcracks were observed close to the fracture surface (the maximum stress region). This shows the dependence of highly localized graphitic corrosion on the stress concentration. Figure 32 in the Appendix C shows typical localized penetration and microcracks in the centrifugally case, cast iron specimens tested.

Evaluation of the Graphitic Corrosion

Table 11 gives the exposure times with the maximum and average penetration and penetration rates. This provides data for three values of static stress without applied voltage for both materials A and B. The exposure time to failure decreases as we increase the static stress and the maximum and average penetration rate increases. Figures 28 and 29 show the variation of the maximum and average corrosion rate versus the level of static stress. Both diagrams show a critical static stress value above which the maximum and average corrosion rates are catastrophically accelerated. Up to the critical stress, which is about 70 percent of the tensile strength of the material, the maximum penetration rate is about 6.5 times higher than the average

Table 11. Exposure Times to Failure, Maximum and Average Penetrations and Penetration Rates for Three Stress Values with No Impressed Current, of Material A and Material B of Phase III Experiments

Conditions	Exposure Time (Days)		Penetration (inches$\times 10^2$)				Penetration Rate (in$\times 10^2$/day)			
			Maximum		Average		Maximum		Average	
	A	B	A	B	A	B	A	B	A	B
40,000 psi No current	41	67	3.25	7	1.80	3.65	.08	.105	.044	.054
Average	54		5.13		2.73		.09		.05	
55,000 psi No current	39.5	34	5	2.95	2.1	1.7	.127	.104	.051	.057
Average	36.75		4		1.9		.116		.054	
65,000 psi No current	.6	15	.3	3.25	0	.9	q.5	.250	--	.066
Average	7.8		1.77		.9		.375		.066	

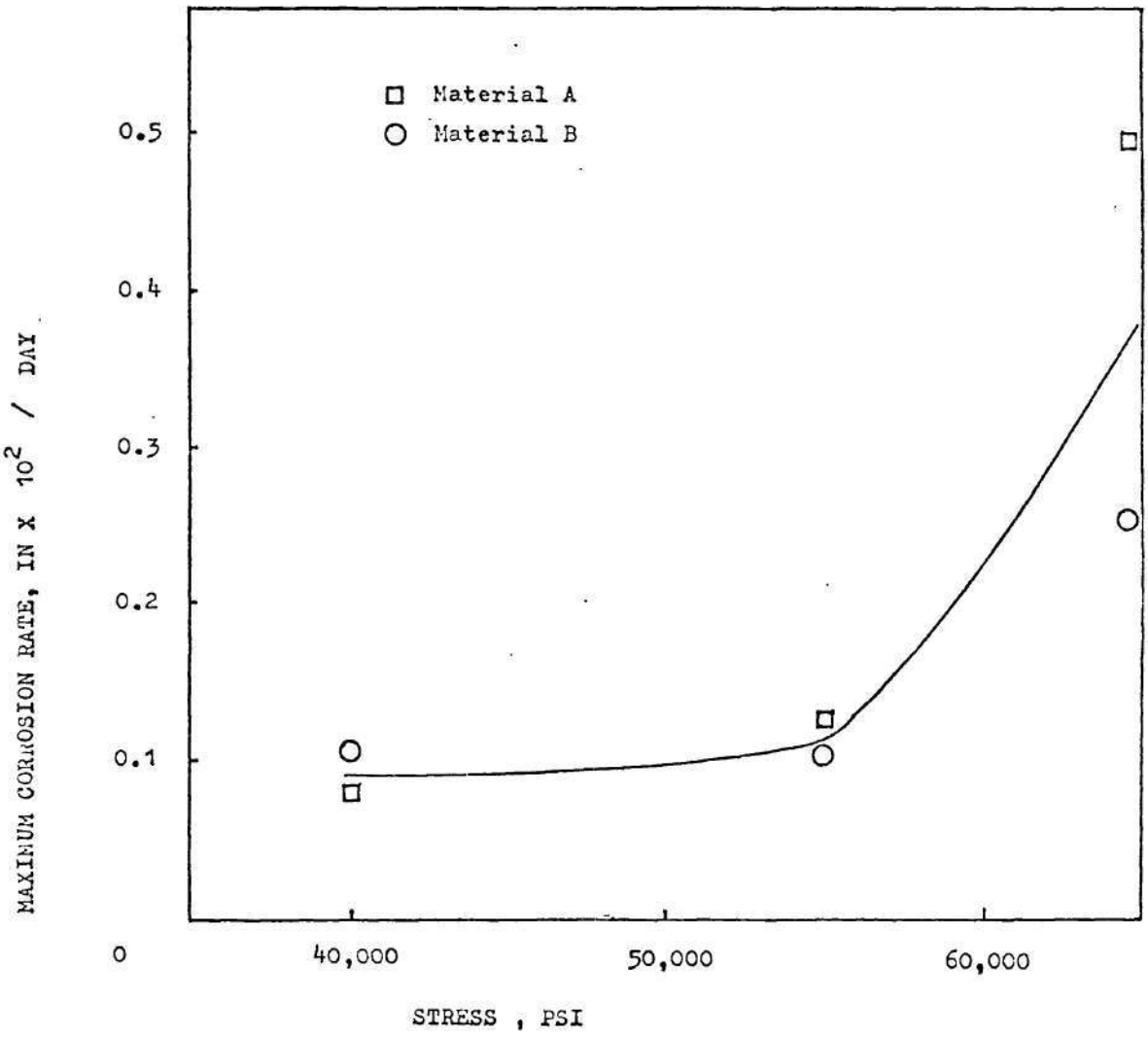

Figure 28. Maximum Penetration Rate Versus Stress for Material A and B

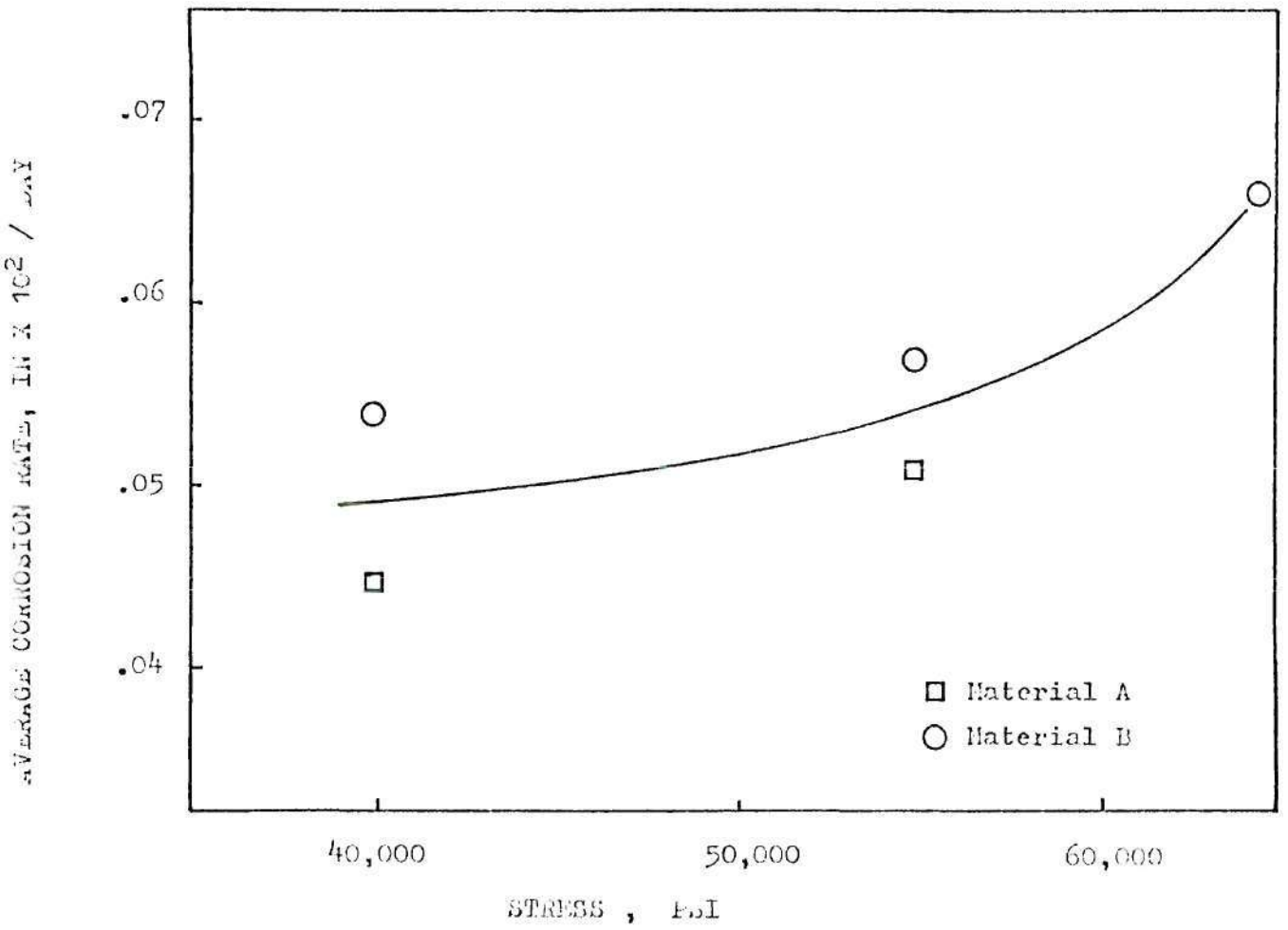

Figure 29. Average Penetration Rate Versus Stress for Materials A and B

penetration rate. Above the critical stress the corrosion rate of maximum penetration became more than twenty times greater. This data verifies that the increase of static stress has a greater effect on the maximum than it does on the average corrosion rate and stress can accelerate the graphitic corrosion rate locally to very high values.

Table 12 gives the time of exposure with the maximum and average penetration and penetration rates for three values of static stress, under applied potential, for both materials A and B. These results are in agreement with the results of Table 11 but show a much higher maximum and average penetration rate which is a result of the applied potential. Figures 30 and 31 give the variation of these rates with the stress. The same value for the critical static stress, 70 percent of the tensile strength value, was found as in the previous experiments.

Table 12. Exposure Time to Failure, Maximum and Average Penetrations and Penetration Rates for Three Stress Values with an Impressed Current, of Material A and Material B of Phase III Experiments

Conditions	Exposure Time (Days)		Penetration (inches$\times 10^2$)				Penetration Rate (in$\times 10^2$/day)			
			Maximum		Average		Maximum		Average	
	A	B	A	B	A	B	A	B	A	B
40,000 psi Current	8	9.25	7.68	10.30	5.06	5.86	.96	1.113	.632	.633
Average	8.63		9		5.46		1.04		.632	
55,000 psi Current	4	3	4.5	3.47	2.58	1.93	1.125	1.157	.645	.643
Average	3.5		4		2.255		1.141		.644	
65,000 psi Current	.3	1.7	.6	2.43	--	1.16	1.49	1.427	--	.685
Average	1		1.51		1.16		1.46		.685	

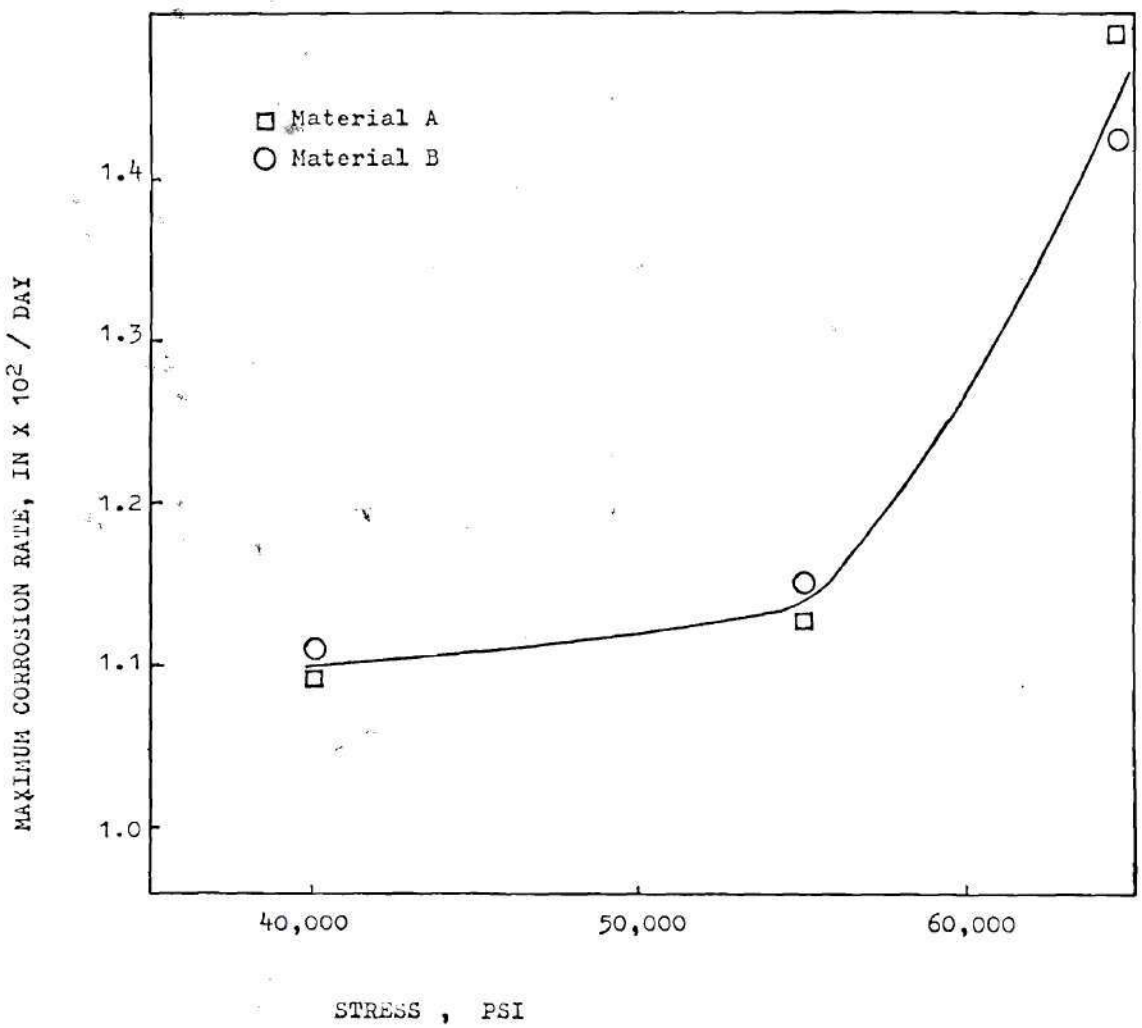

Figure 30. Maximum Penetration Rate Versus Stress (with Applied Potential of 0.2 V) for Materials A and B

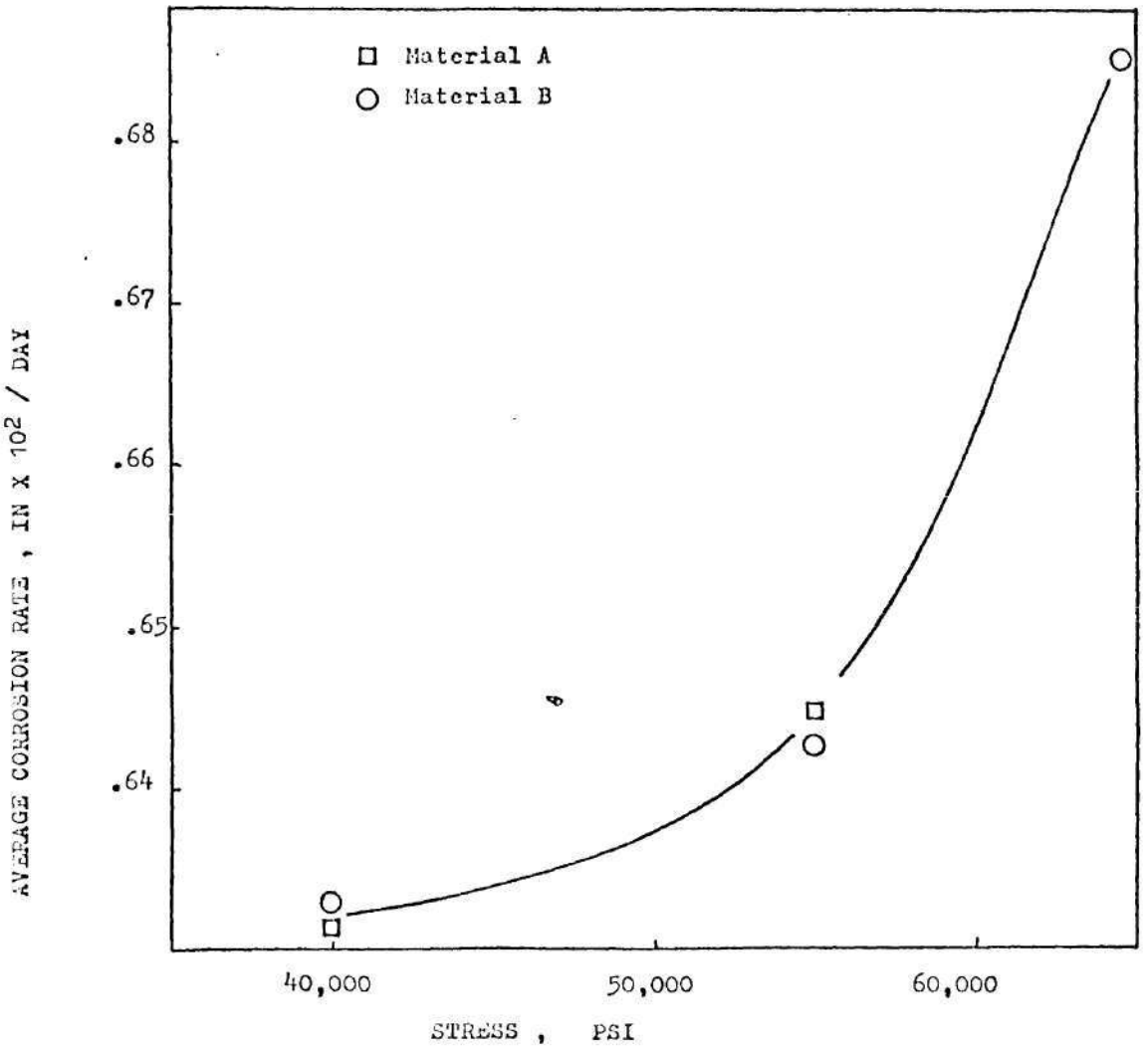

Figure 31. Average Penetration Rate Versus Stress (with Applied Potential of 0.2 V) for Materials A and B

CHAPTER V

CONCLUSIONS

1. Residual stresses substantially increase the normal graphitic corrosion rate with a subsequent decrease in the time to failure by reducing the mechanical strength of the material. Even more severe attack occurs if stresses are combined with an impressed current.

2. Static stresses applied to centrifugally cast, cast iron can develop a graphitic corrosion rate 50 times higher than normal graphitic corrosion, increasing up to 60 times greater with the presence of modest residual stresses. When static stress, or static stress plus residual stress, are combined with an impressed current, corrosion rates more than 100 times the normal graphitic corrosion rate readily occur.

3. As the static stress is increased a critical stress (approximately 70 percent the tensile strength) is reached where the corrosion rate and especially the maximum penetration corrosion rate increases catastrophically.

CHAPTER VI

RECOMMENDATIONS

1. Evaluate the effect of alloying and casting variables on the graphitic corrosion of ductile cast iron with the potential of developing graphitic corrosion resistent ductile iron for gas distribution line applications.

2. Investigate the effects of static and cyclic stress on graphitic corrosion of ductile cast iron.

3. Relate the effects of static stress on graphitic corrosion of centrifugally cast, cast iron in corrosive soils, such as Acadia clay and Lake Charles clay.

APPENDICES

APPENDIX A

LOAD CALCULATION

The forces and reactions on the specimen are represented in the following diagram:

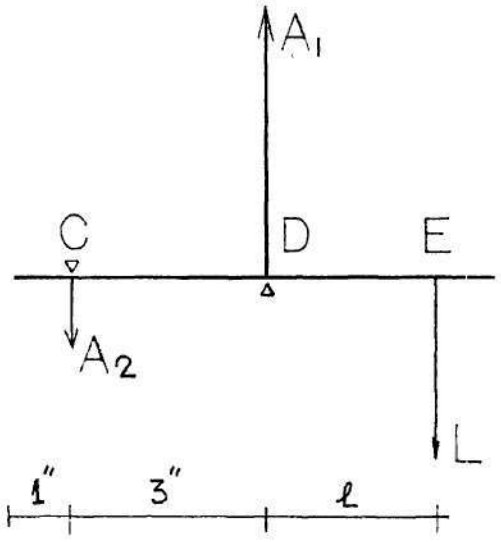

$A_1 = A_2 + L$ $\qquad A_2 = \frac{\ell L}{3}$

$3A_2 = \ell L$ $\qquad A_1 = L(\frac{\ell}{3} + 1)$

where L = the load

ℓ = distance between load and point D

A_1, A_2 = reactions on points C,D.

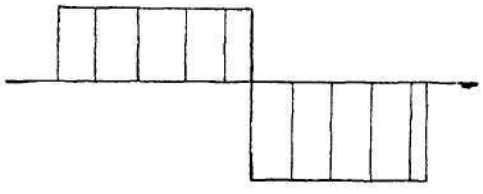

Force diagram

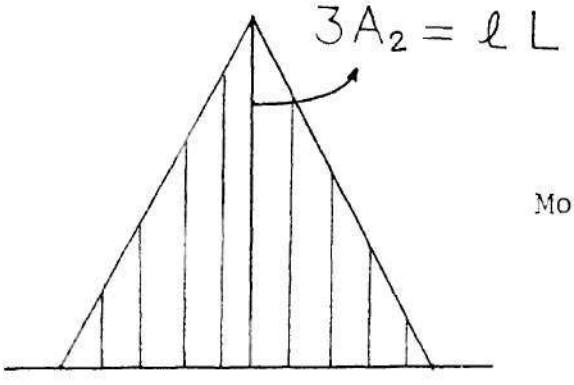

Moment diagram

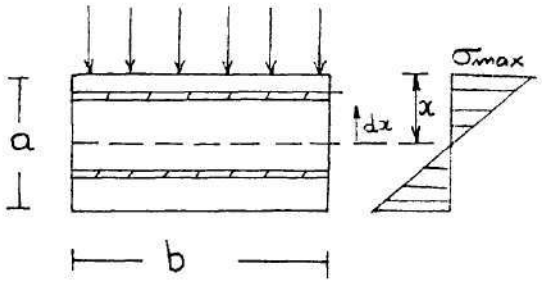

where σ_{max} = max stress
a = thickness
b = wideness

Examining the cross-section at the maximum moment layer, it is derived that:

$$\ell L = \int_{o}^{a/2} 2 \, x \, [\frac{x}{a/2} \sigma_{max}] b dx \qquad \text{or}$$

$$\ell L = \frac{4}{a} b\sigma_{max} \frac{x^3}{3}\Big|_{o}^{a/2} \qquad \text{or}$$

$$\ell L = \frac{4b}{a} \sigma_{max} \frac{a^3}{8} = \frac{\sigma_{max} a^2 b}{6} \text{ and finally}$$

$$\sigma_{max} = \frac{6\ell L}{a^2 b}$$

APPENDIX B

POURBAIX DIAGRAM FOR IRON

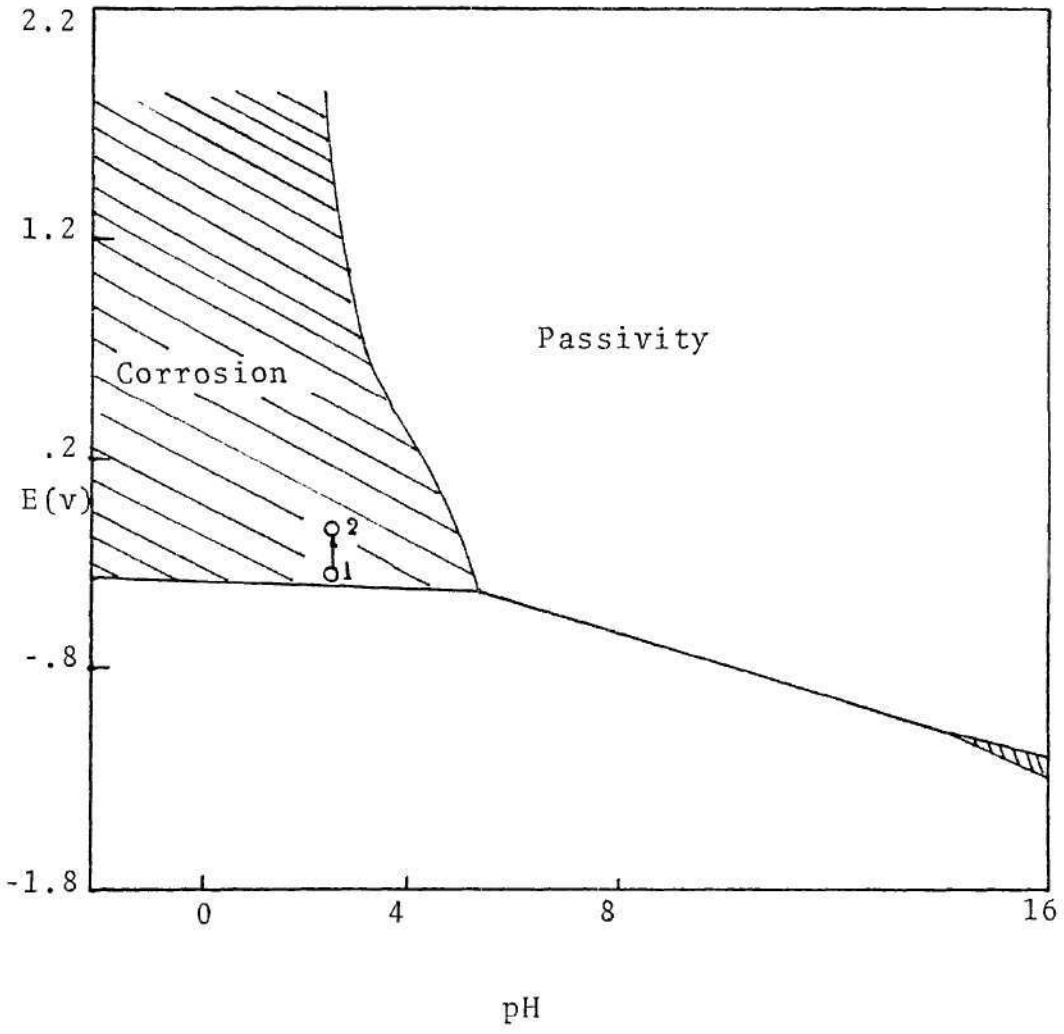

APPENDIX C

PHOTOMICROGRAPHS OF THE GRAPHITIZED SPECIMENS UNDER STRESS

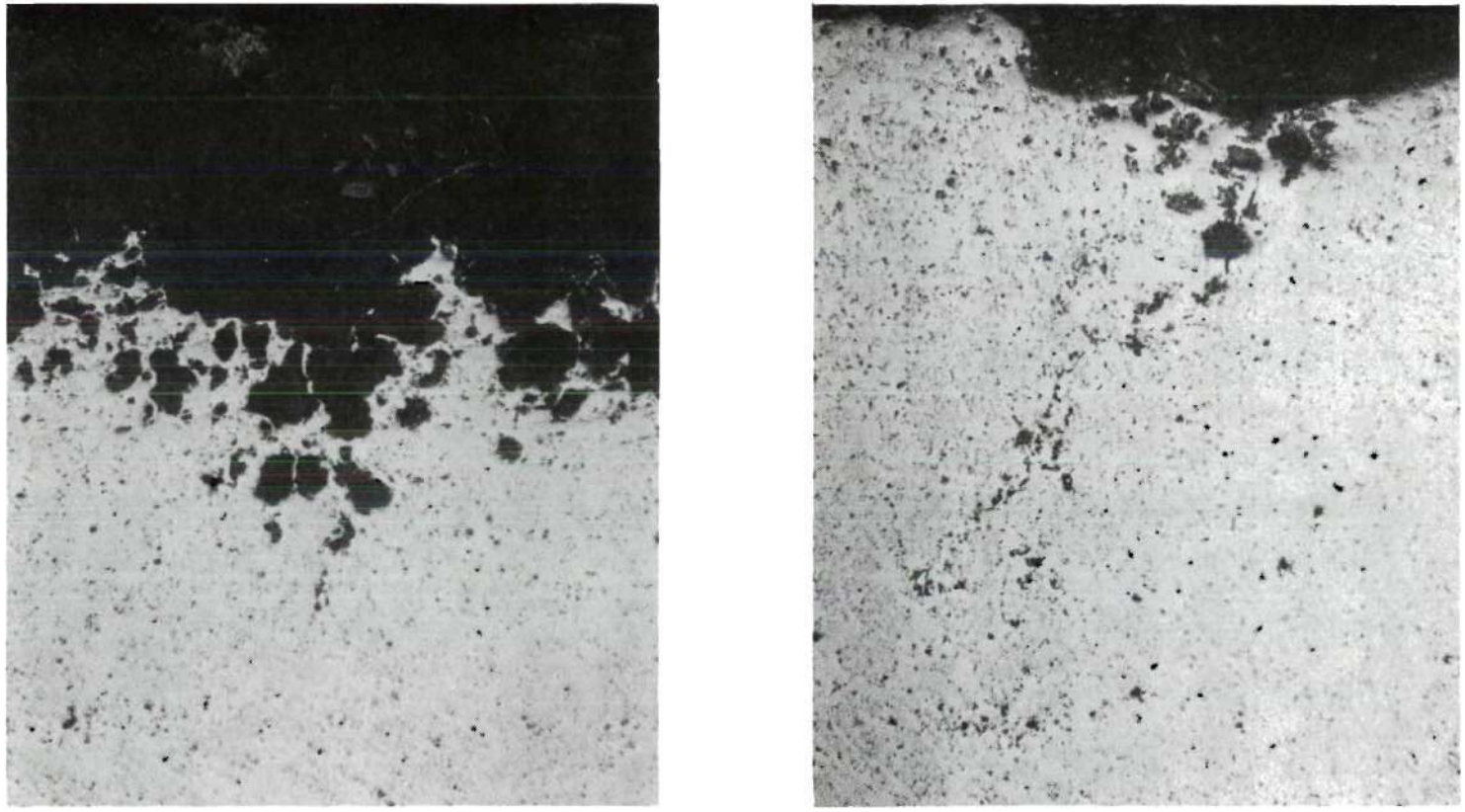

Figure 32. (a) and (b) 65X Magnification. Unetched--Photomicrographs of Two Typical "Finger-Like or Fissure" Graphitization Attacks

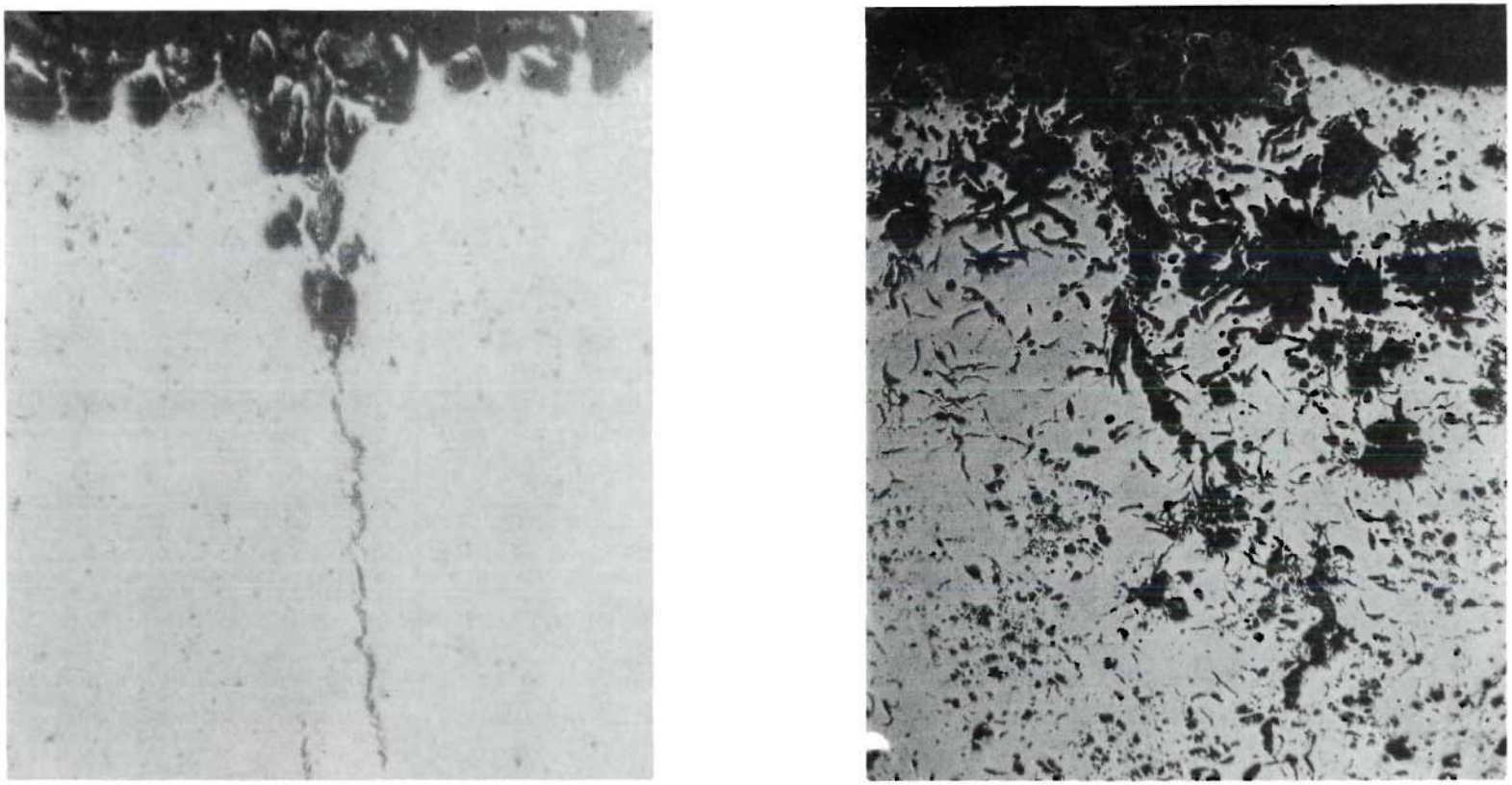

Figure 32. (c) and (d) 100X Magnification. Unetched--Photomicrographs of Two Cracks Close to Fracture Surface

BIBLIOGRAPHY

1. ASM, Metals Handbook, Vol. I (1975), p. 349-365, 402-403, Vol. 10 (1975), p. 80, 176-177, 182-183, 190-191, 199, 332.

2. W. A. Wesley, H. R. Copson, F. L. LaQue, "Graphitic Corrosion of Cast Iron," Metals and Alloys, Vol. 7 (Dec. 1936), 325-329.

3. F. L. LaQue, "The Corrosion Resistance of Dustile Iron," Corrosion-National Association of Corrosion Engineers, Vol. 14 (Oct. 1958), p. 485-492.

4. E. C. Sears, "Soil Corrosion Resistance of Dustile Iron Pipe," Proceedings 24th Conference, NACE, (1968), p. 533-540.

5. G. Bianchi, F. Mazza, E. Sivieri, "Electrochemical and Metallurgical Factors in Cast Iron Graphitization in Sea Water," 6th International Congress on Metallic Corrosion, Technical Section N.I. (1975).

6. F. L. LaQue, "Corrosion Characteristics of Ductile Iron," J. American Water Works Association, Vol. 56, No. II (Nov. 1964), 1433.

7. M. Romanolf, "Exterior Corrosion of Cast-Iron Pipe," J. American Water Works Association, Vol. 56, No. 9 (Sept. 1964) 1129.

8. Cast Metals Handbook, 3rd Edition, (1944), p. 341.

9. Lefferd B. Haughwont, "Centrifugal Casting Processes," Castings, Production Engineering Series, (1971), p. 109-116.

10. J. P. Scholes, "Properties Affecting the Performance of Iron Castings Under Static Loads," Conference on Engineering Properties and Performance of Modern Iron Castings, University of Technology, Loughborough, (1970), p. 80-82.

11. G. N. J. Gilbert, "Behavior of Cast Irons Under Stress," Conference of Engineering Properties and Performance of Modern Iron Castings, University of Technology, Loughborough, (1970), p. 39-73.